Synthesis and Characterizations of ZnO Thin Films and Nanostructures by Modified Aqueous Chemical Growth Method for Sensor Applications

Surya Prakash Ghosh

Department of Physics and Astronomy
National Institute of Technology Rourkela

Dedication

To my Parents

The reason of what I become today

Thanks for your great support and continuous care.

To my sweet siser

A sister is a little bit of childhood that can never be lost,

I am really greatful to you,

You have been my inspiration throughout the journey.

To my brother and Friends.

Synthesis & Characterizations of ZnO Thin Films and Nanostructures by Modified Aqueous Chemical Growth Method for Sensor Applications

A THESIS SUBMITTED FOR THE AWARD OF THE DEGREE

of

Master of Technology (Research)

by

SURYA PRAKASH GHOSH

ROLL No-612PH302

Under the supervision of

Dr. Jyoti Prakash Kar

Department of Physics and Astronomy
National Institute of Technology Rourkela
Rourkela-769008, Odisha, India

December 2015

DECLARATION BY THE CANDIDATE

I declare that the thesis entitled ***"Synthesis and Characterisation of ZnO Thin Films and Nanostructures by Modified Aqueous Chemical Growth Method for Sensor Applications"***, is based on my own research work conducted under the supervision of **Dr. Jyoti Prakash Kar** at NIT Rourkela, Odisha, India, approved by Masters Scrutiny Committee.

I further declare that to the best of my knowledge that the thesis does not contain any part of work which has been submitted for the award of any degree either in this Institute or in any other University/Deemed University without proper citation. I have confirmed to the norms and guidelines given in the ethical code of conduct of the Institute.

Surya Prakash Ghosh

CERTIFICATE

This is to certify that the thesis entitled, "**Synthesis & Characterizations of ZnO Thin Films and Nanostructures by Modified Aqueous Chemical Growth Method for Sensor Applications**" has been submitted by **Mr. Surya Prakash Ghosh** for the award of the degree of **Master of Technology (Research)** to the National Institute of Technology Rourkela, Rourkela is a record of bonafide research work carried out by him under my guidance and supervision.

In my opinion, the thesis has reached the standard fulfilling the requirements of all regulations related to the degree. The results contained in this thesis have not been submitted in part or full, to any other University or Institute for the award of any degree or diploma.

Dr. Jyoti Prakash Kar
Department of Physics and Astronomy
National Institute of Technology Rourkela
Rourkela-769008

ACKNOWLEDGEMENT

The completion of this thesis work is an outcome of the contribution from a lot of people, who helped me either directly or indirectly deserve acknowledgment. The past 3 years at National Institute of Technology Rourkela, was the paramount learning experience for me. I am highly indebted to Prof. S. K. Sarangi, Hon'ble Director, NIT Rourkela for providing required facilities for my research work. I would like to express my special appreciation and acknowledgement to my supervisor Dr. Jyoti Prakash Kar; you are a tremendous mentor for me. I would like to thank you for encouraging my research and allowing me to grow as a researcher. Your advice on both research as well as on my career are priceless.

I express my hearty thanks to my Masters of Scrutiny committee members Dr. D. K. Bisoyi, Dr. D. Behera, Dr. B. Ganguli, Dept. of Physics and Astronomy and Dr. S. K. Pratihar, Dept. of Ceramic Engineering, NIT Rourkela, for valuable suggestions to improve the quality of research.

I express my sincere acknowledgement to Prof. J. M. Myoung, Department of Materials Science and Engineering, Yonsei University and also to Dr. T. I. Lee, Department of Bio-Nanotechnology, Gachon University, Republic of Korea, for their hospitality during my visit to Korea and providing facilities for carrying out my research work. I am thankful to Dr. P. Pal and Mr. A. Ashok, Dept. of Physics, IIT Hyderabad for helping me to characterize the samples at IIT Hyderabad.

I would like to express a deep sense of gratitude towards my labmates Mr. Kailash Chandra Das and Mr. Nilakantha Tripathy for their continuous encouragement,

co-operation, and suggestion in my research work. Without them it would be impossible for me to complete the work.

I would also like to thank other labmates, Archana, Subhra, Neeha, Sandeep, Agnish, and Ravi for helping me in my research work as well as creating healthy environment in Electronic Materials and Devices (EMD) Laboratory. I sincerely thank all research scholars, fellow friends of Dept. of Physics & Astronomy for their support, help during these 3 years. I acknowledge Mr. Radha R. Nayak, Mr. Subhabrata Chakraborty for helping me to carry out XRD and FESEM studies. I whole heartedly thank all the faculty members and non-teaching staffs of Dept. of Physics & Astronomy for their kind cooperation during the entire period.

I would like to acknowledge Department of Science and Technology (DST) India for providing fellowship from Indo- Korea project (INT/Korea/P-16/2013) during my research work.

Lastly, I would like to thank my grandparents for all they taught me. Especially, I would like to express my sincere gratitude to my beloved parents: their hard work and moral support, which have not only inspired me but also given me strength throughout my whole life. I thank my family for always being there for me and for supporting me in the decisions that I make …….

Surya Prakash Ghosh

ABSTRACT

In recent years, there is a great demand on the development of portable, low cost, low power operated high performance sensors for medical diagnosis, defence, space, agriculture and industrial applications. Remarkable research on the fabrication of the semiconducting metal oxide (ZnO) based resistive sensors are currently being drawn considerable continuous attention for sensor fabrication because of its semiconducting nature, direct and wide bandgap (3.37 eV), ease of fabrication, low cost, non toxic nature, high temperature stability and CMOS compatibility.

In order to achieve low cost portable sensors, room temperature operated devices are highly preferred. However, lowering of operating temperature significantly reduces sensing activities. In order to enhance the performance of the room temperature operated sensors, the enhancement in the surface area of the active material is an alternate approach. In this research work, ZnO thin films and nanostructures were fabricated on CMOS compatible silicon substrate. Prior to the growth of the nanostructures, growth condition of seed layer was optimized by varying the sputtering parameters. Post-deposition rapid thermal annealing was carried out for various conditions for improving the crystallinity of the seed layer. The films annealed for higher duration has shown porous morphology. Afterwards, various types of nanostructures such as nanowires, nanorods, nanoplatelets and network like porous structure were synthesized by varying the parameters of limited area heating of aqueous chemical method. Nanoplatelets/flakes like structures were appeared as a result of incorporation of aluminium nitrate in the zinc nitrate and hexamethyltetramine precursor. Electrical contacts on the samples were fabricated by thermal evaporation of aluminium by adopting shadow mask technique. The sensitivity of ammonia and UV on/off current ratio was calculated by performing current-time measurements. The decay time constant of UV detection are estimated from fitting of exponential data. Among different samples ZnO network like porous structures have shown better sensing property.

TABLE OF CONTENTS

LIST OF FIGURES

Chapter- 1

Introduction

1.1 Overview

In recent years advancement in sensor technologies are driven by fabrication of high quality sensor materials, microelectronic hybrid circuits [1-4], modern signal processing methods [5-6] and the advances in miniaturized encapsulation [7-11]. Worldwide research is being conducted to improvise effective ways on the development of portable, low cost, low power operated high performance sensors for various applications such as medical diagnosis, defence, space, agriculture and automation in industries [12-13]. With the progression in technology, there is a demand on highly precise and responsive sensors from safety point of view. The current technology demands the miniaturizations of electronic devices, which can be possible by monolithic integration of sensors on silicon substrate. In order to develop a sensor of better efficiency, it must satisfy some parameters such as high accuracy, high sensitivity, longevity, high response rate. Broadly, there are two kinds of sensors: active and passive. The active one can convert one form of energy directly into another without the need of an external source, while the passive one is not able to convert the energy directly, but it checks the energy or the excitation from another source [14]. Sensors can also be classified according to their objectives such as pressure and force sensors, sensors for level, speed sensors, sensors for acceleration, sensors for vibrations, sensors for magnetic field, sensors for vacuum, sensors for displacement, temperature sensors, humidity sensors, gas sensors, biosensors, sensors for radioactive radiation. In addition, categorization of the sensors is also based on the nature of the sensing material such as metal oxide, ceramic, polymers and composites. The sensitivity of the sensors greatly depends on the surface area of the sensing material, surface functionalization, design of electrode and temperature of the operation etc. Based on the requirement, sensing materials are fabricated in different forms such as bulk, thin films and nanostructures for sensor applications.

1.2 Motivation and historical background of sensors

Measurement of sensing behaviour, based on variation in resistance, was first reported in 1950s by two scientists named Brattain and Bardeen [15]. Later, Heiland revealed the modification in the semiconducting properties of metal oxides with a variation in the partial pressure of gases like oxygen in the surrounding atmosphere [16]. During 1960, Seyama revealed that the sensing behaviour of gas can be measured by using metal oxide thin film as a sensing layer along with simple electrical devices. The response of the detection system to propane was about 100 times higher compared to the thermal conductivity detector used at that time [17]. Later, in 1967, Shaver has illustrated the modification of sensing behaviour of oxide semiconductors by the addition of noble metals (e.g., Pt, Pd, Rh) [18]. After that discovery, research on sensitivity of semiconductor has been intensified. Taguchi was the first person to fabricate and patent chemoresistive gas sensor in 1970 for practical applications using tin dioxide as the sensitive material [19]. Semiconductor based gas sensors have drawn noteworthy attention and became one of the most active research areas among sensor community since 1980. This leads to a rapid development of new sensing materials in order to achieve high performance sensors with high sensitivity and selectivity, faster response, together with low power consumption and high device reliability. Monolithic integration of sensors is under high demand for number of applications in versatile fields, which includes industrial emission control, household security, vehicle emission control, environmental monitoring, agricultural and biomedical applications [20]. In recent years, advances in semiconducting sensing materials merely depend on the scope provided by nanoscale technology. Moreover, emerging nanotechnology assures remarkable development in sensor designs and capabilities. Thus, reliable and robust technologies are highly required in order to meet the enviable performance criteria like lesser power consumption, room temperature operation, low cost material synthesis, ease of fabrication with better selectivity and sensitivity.

1.3 Classification of gas sensors

Basically, sensor is a device able to interface the chemical, physical and biological world with that of electronics by change in parameters such as refractive index, dielectric constant,

shape, mass, carrier concentration etc. According to IEC (International Electrotechnical Committee) “Sensor is the primary part of a measuring chain which converts the input variable into a suitable signal for measurement” [21]. The active element of a sensor, which senses and converts one form of energy to another, is termed as transducer. With the advances in micromachinery and easy-to-use microcontroller platforms, the uses of sensors have expanded beyond the traditional fields of temperature, pressure or flow measurement. In general, based on the operating principle and design, a sensor can possess high sensitivity, high precision, reproducibility and high response rate. On the basis of working principle, the sensors are broadly categorized into physical sensor and chemical sensor as shown in fig. 1.1. The gas sensor comes under the category of chemical sensor.

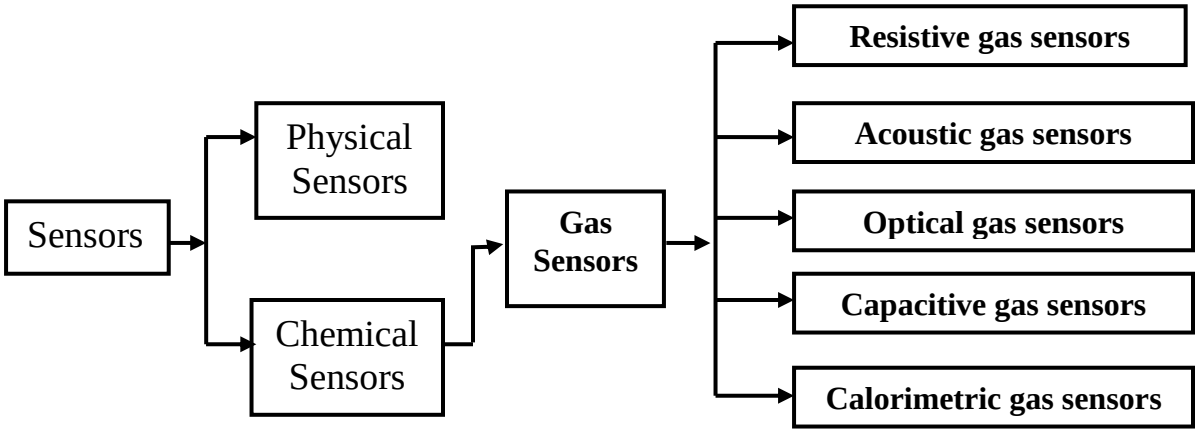

Fig. 1.1 Classification of sensors [22-25]

Chemical sensors, based on change in resistance, are termed as resistive sensors. A resistive sensor is based on a sensitive material, in form of bulk/thin film/nanostructure upon which the molecular recognition process takes place. The analyte recognition process occurs either at the surface of the sensing element or in the bulk of the material, leading to a concentration-dependent change in electronic property that can be transformed into an electrical signal. This simple transduction mechanism governs the fabrication of devices with different configurations. In comparison to other sensors like electrochemical and optical, resistive sensors are advantageous due to its small size, low cost, longer lifetime. The resistive gas sensors are

further classified according to the sensing material such as metal oxide and conductive polymer [23]. However, metal oxide gas sensors can be used in high temperature application.

1.4 Ammonia sensors

Ammonia, a chemical having a chemical formula of NH_3, is widely used in numerous major components in fertilizer manufacturing, household cleaners, fermentation industry, pharmaceuticals and is also used as a refrigerant irrespective of its highly sorptive, toxic, and potentially harmful nature. It is produced by both nature and human being. The worldwide emission of ammonia per year, estimated by the European community commission for environment and quality of life, was 20–30 Tg in 1980 [26]. Other investigations, summarized by Warneck [27], were estimated the values between 22 and 83 Tg.

1.4.1 Sources of ammonia

- As a natural gas in atmosphere
- Direct or indirect emission by human activity
- Fertilizer like ammonium and nitrate salts
- Through plants nitrification i.e. bacterial nitrogen fixation
- Ammonification, a series of metabolic activities that decomposes organic nitrogen like manure from agriculture and wildlife
- Combustion, both from chemical plants and motor vehicles. The total emission of ammonia from combustion is about 2.1–8.1 Tg/year [28]
- Surface water, normally seas and ocean occasionally act as an ammonia source [29, 30], alkaline rain water etc. [31]

1.4.2 Necessity for ammonia sensor

Ammonia is directly or indirectly associated with human beings in various ways such as in earth atmosphere, nitrogen cycle in plants, chemical industries. It is the building-block for the synthesis of many pharmaceuticals as well as utilized in many chemical products. It is equally caustic and hazardous in nature. Its effect on living beings is detrimental and in some cases fatal. Researchers have shown that ammonia has possessed lowest global warming and ozone depleting potential compare to other traditional refrigerants [32]. Thus, ammonia is used as a refrigerant in ice making plants and cold storages at several places. This is the one major source of ammonia gas emission. Furthermore, detection of lower concentration of ammonia is very

important from the view of chemical pollution during the production of silicon devices in clean rooms [33]. There is a great probability that human beings and livestock's residing in nearby places may be subjected to the emissions of ammonia due to leakage. Leakage of ammonia can occur due to different reasons such as faulty instrumentation, ageing machineries, defective connections etc. Excess emission of ammonia to the environment may cause severe disorders to the living entities. Ammonia and ammonium hydroxide are corrosive and can rapidly penetrate the eye, nose or mouth may cause permanent injury. Exposure to high concentrations of ammonia in air causes immediate burning of the nose, throat and respiratory tract. Also it can cause bronchiolar and airway destruction resulting in respiratory distress or failure. Ammonia inhaled in lower concentrations for prolonged period results in coughing, olfactory fatigue, ulcer and throat irritation. There are certain standards which dictate the maximum exposure limit to ammonia gas, all the work places are bound to abide this limit. The Permissible Exposure Limit for ammonia, set by Occupational Safety and Health Administration (OSHA), is 50 parts per million (ppm) averaged over an eight hour work day [34]. Hence, development of room temperature operated ppm level ammonia sensor is highly essential.

1.4.3 Resistive type metal oxide ammonia sensor

There are different types of ammonia sensors such as catalytic ammonia sensors, conducting polymer ammonia sensor, optical gas analyzers, spectrophotometric ammonia sensor, acoustic ammonia sensor and capacitive ammonia sensors [35-36]. Metal oxides generally used as sensitive layer in resistive devices comprise of binary oxides such as SnO_2, ZnO, TiO_2, WO, CuO, Fe_2O_3, In_2O_3, and CdO [40-49]. However, metal oxide based ammonia sensor draws considerable attention because of its simplicity, low cost and high temperature stability as well as longevity. Although responsive and consistent NH_3 sensors have been fabricated based on ZnO nanostructures, they require high operating temperatures (typically > 250 °C) to trigger the adsorption and desorption processes of NH_3 [37-40, 50], which results in high energy consumption and limits their use in low temperature applications. In addition, the size and the cost of the sensor are also increased due to the extra heating arrangements. However, lowering of operating temperature significantly reduces sensing activities. In order to enhance the performance of the sensors (operated at room temperature), enhancement in the surface area of the active material is an alternate approach. Thus, sensitive detection of NH_3 at room temperature is still highly required in order to reduce the size and its cost. Numerous researches have been

conducted for years in order to alleviate the shortcomings of the previous ammonia sensors and coming up with improved technologies.

Metal oxide semiconductor is tremendously admired as low cost sensors, which work on the principle of reversible redox reaction between the sensor material and the analyte. Wide spread structural, physical, chemical properties and functionalities of metal oxides make them most assorted and largest class of materials. The important characteristic properties of a reliable ammonia sensor are fast sensor response and recovery, superior mechanical strength, long operating life, low cost, small size and easy to handle. Over the last few decades, researchers around the world have been able to meet this demand with the use of advanced technology and novel materials.

1.4.4 Ammonia sensing behaviour of ZnO

Ammonia sensors can be fabricated using various metal oxides as discussed in above section. However, they suffers from various limitations such as PdO has poor selectivity, SnO_2 based sensors require high operating temperature; WO_3 requires nobel metal additives like Pt, Au, Ag [51-53]. In addition, conducting polymers have also been used as sensor materials, which are superior in terms of fabrication, which has tunable conductivity, structural variability, room temperature operatibility and low cost. However, they are thermally unstable and moisture sensitive. Thus, among different sensing materials, ZnO has been given key importance because of its chemical stability, low cost, ease of synthesis and biocompatibility.

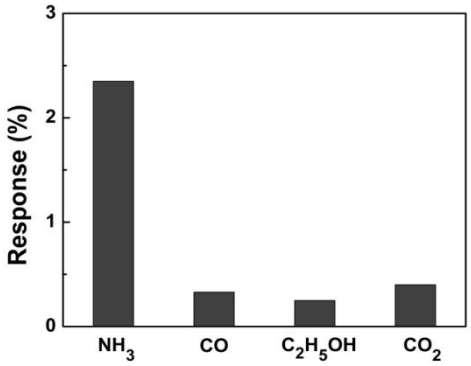

Fig. 1.2 Higher selectivity of the ZnO based NH_3 sensor [54]

Among different gases such as carbon dioxide, ethanol, carbon monoxide and ammonia, the selectivity of ammonia is higher for ZnO based sensor as shown in fig. 1.2 [54]. On exposure to ammonia, a remarkable decrease in the resistance of the ZnO based sensor takes place [55] which is due to generation of more number of free carriers as a result of surface interaction.

1.5 ZnO as an UV detector

The bandgap of ZnO (3.37 eV) falls in the intermediate region between visible and UV light. ZnO is preferred for UV detector due to its high on/off current ratio, fast response and recovery, large photoresponse current and wavelength selectivity [56-58]. UV lights are used in food processing, sterilization of medical equipment, research laboratories, semiconductor processing industry etc., where an installation of UV detector is highly required. In addition to sensor applications ZnO is also highly desired for thin film transistors, light emitting diodes, solar cells, surface acoustic wave and energy harvesting devices [59-60]. Therefore, synthesis of ZnO nanostructures is under active investigation for the development of next generation of robust electronic devices.

1.6 Historical background of ZnO

Research works on ZnO material started as early as 1920's with the first utilization of ZnO for its semiconducting properties as a detector in radio sets, in which a thin copper wire, known as "cat's whisker", is placed in contact to sensitive spots on a ZnO crystal [61]. Zinc oxide is also known as "Lu-Gan-Stone" in China, and has been used in medical treatment for quite number of years in China. Since 1950, there were number of reviews on electrical [62] and optical properties like n-type conductivity [63], absorption spectra and electroluminescence decay parameter of ZnO. Damen and Porto in 1960 has successfully studied the Raman effect of ZnO and reported about the phonon energy associated with zinc oxide [64-65].

Since 1960s, ZnO thin films are actively synthesized by various routes because of their applications as sensors, transducers and catalysts. Groenen have used thermal plasma to deposit surface textured ZnO films. Liping Dai et al., (2008) have prepared a–b axis orientation ZnO film on silicon (100) substrate by a single source chemical vapor deposition technique. Doyoung Kim et al., have investigated the low pressure chemical vapour deposition of Al doped ZnO thin film for transparent electrode of thin film solar cell.

In the last few decades, especially since the nanotechnology initiative led by the US, study of one dimensional (1D) materials has become a leading edge in nanoscience and nanotechnology. With reduction in size, novel optical, chemical and sensing properties are introduced, which are supposed to be the result of surface and quantum confinement effects [66].

ZnO is a multifunctional material that has a diverse group of growth morphologies, such as nanocombs, nanorings, nanohelixes/nanosprings, nanobelts, nanowires and nanocages [67]. ZnO with nanowire-like shapes are the ideal system for studying the transport process in one-dimensionally (1D) confined objects, which plays a vital role not only for understanding the fundamental phenomena in low dimensional systems, but also for developing new generation sensor devices with low cost and high performance. A lot of work on deposition of high quality nanostructures and thin film of ZnO has been successfully accomplished by developing techniques like vapour liquid solid (VLS), metal-organic chemical vapour deposition (MOCVD), spray pyrolysis, electrodeposition and radio frequency (RF) magnetron sputtering [68]. Overall most of the research in 1980's was attempted to resolve the issues concerning with lack of satisfactory material for device fabrication. In 1990's, newer growth methods were used including pulsed laser deposition (PLD) and molecular beam epitaxy (MBE). Sandana et al., (2009) compared the properties of ZnO nanostructures grown on Si (111) and c-plane sapphire (c-Al_2O_3) substrates using three different growth processes: MOCVD, PLD and physical vapor transport (PVT) [69-70]. Though research on ZnO has started many decades ago but in the current technological arena, many academic and government laboratories, companies and NGO's across the globe are deeply engaged to exploit the various nano form of ZnO such as nanohelix, nanoflowers, nanobelts, naotubes, naoflakes etc. due to its versatile applications in the futuristic emerging technology [70].

1.7 Crystal and surface structure of ZnO

Zinc oxide which naturally occurs as the mineral zincite is a key technological material. Polar symmetry along the hexagonal axis of ZnO is responsible for the origin of the piezoelectricity and spontaneous polarization making it suitable candidate for mechanical actuators and piezoelectric sensors. In addition, this polarity contributes to the crystal growth and etching in ZnO. Generally, zinc oxide crystallizes in two main forms, hexagonal wurtzite and cubic zinc blende. The wurtzite structure is obtained only at optimum pressure and temperature, which is the most thermodynamically stable phase of ZnO as explained by Hartree-Fock [71-77]. The zinc (Zn) atoms are tetrahedrally co-ordinated to four oxygen (O) atoms, with the oxygen anions occupying the octahedral sites. ZnO thin films show n-type semiconducting behaviours [78]. Intrinsic native defects such as oxygen vacancies (V_O) or Zn interstitials (Zn_i) are

responsible for the naturally occurring n-type character in ZnO. However, there is still a great deal of debate over which of these two defects is the dominant cause of the n-type conductivity [79]. Some researchers have suggested that hydrogen in the environment act as shallow donor. Based on density functional theory calculation, it has been shown that hydrogen forms a strong bond with O in ZnO and act as shallow donor [80].

1.8 Growth mechanism of ZnO nanostructures

Overally the larger sensing area is one of the key factors for better performance of sensors. Sensing area can be enhanced by growth of various types of nanostructures on CMOS compatible substrates such as silicon, which is highly preferred for the fabrication variety of electronic materials.

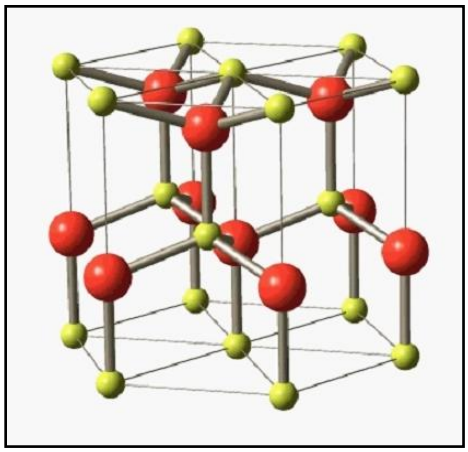

Fig. 1.3 Crystal structure of ZnO [77-80]

In order to grow nanostructures of various morphology for sensor applications a good quality seed layer is highly essential. Varieties of growth techniques are being implemented for deposition of high quality seed layer through of physical and chemical routes, such as pulsed laser deposition, thermal evaporation, chemical vapour deposition and magnetron sputtering [75, 76-78]. Among these techniques, RF magnetron sputtering has several advantages such as low thermal budget, multitarget arrangements, nontoxic, and its ability to produce crystalline films with desired properties [79]. However, there is a chance of deterioration in the film crystallinity due to atomic inter collisions in the plasma or ionic bombardment on film surface during the sputtering, which generally gives rise to the formation of defects in the sputtered films [79, 80]. Hence, in order to enhance the crystallinity and annihilate the defects in the sputtered film, post-deposition heat treatments (rapid thermal annealing) are generally performed. Well aligned

nanostructures can be obtained using crystalline seed layer. In order to enhance the sensors performance, ZnO nanostructures are under active consideration due to their significant properties like high electron mobility, non-toxic nature, high-specific surface area, good chemical and thermal stability under operating conditions [81]. Hence, if the sensors will be integrated with the other electronic components, there will be a possibility for the fabrication of portable, low cost high performance sensing devices through monolithic integration.

Another interesting result of the non-centrosymmetric ZnO crystal structure is its spontaneous polarization and polar face dominated nanostructures [82]. The most common polar surface is the basal plane. The crystal structure of ZnO shown in fig. 1.3 can be described as number of alternating planes composed of tetrahedrally coordinated Zn^{2+} and O^{2-}ions alternatively stack along c-axis. Owing to the positive or negative ionic charges on the surface i.e. the surface is either Zn terminated or O_2 terminated. The oppositely charged ions produce positively charged Zn-(001) and negatively charged O-$(00\bar{1})$polar surfaces, resulting in a normal dipole moment and spontaneous polarization along the c-axis as well as a divergence in surface energy [83]. Due to spontaneous polarization, the position of positive charge is displaced from that of negative charge and the direction of displacement is along [001]. The net result of this spontaneous polarization is a charged (001) ZnO surface. The other two most commonly observed facets for ZnO are $(0\bar{1}0)$ and $(\bar{1}\,\bar{1}0)$, which are non-polar surfaces. Thus, by tuning the growth rate along polar and non-polar surfaces (shown in fig. 1.4) different unique nanostructures such as nanohelix, nanobelts, nanotubes, nanoflakes, nanoplatelets can be obtained.

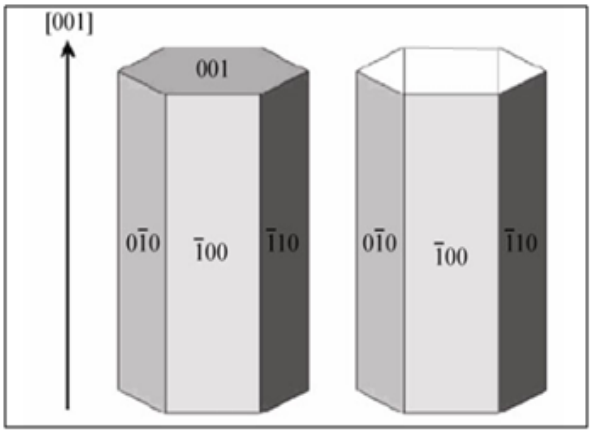

Fig. 1.4 Polar and non-polar surface of ZnO

Zno nanowires and nanorods are obtained as a result of the growth along (002) direction. Nanohelix is obtained due to Zn^{2+} terminated polar surface. A sequential and periodic 60^{o} rotation along six equivalent growth directions in a ordered and equally spaced distance results in the formation of nanohelix [83]. Sequential change in growth direction is induced by electrostatic interaction energy of system. Similarly, ZnO growth along nonpolar direction such as $(2\bar{1}\bar{1})$ and $(\bar{1}\bar{1}0)$ along with high energy polar surface (001) results in the formation of nanobelts. Nanotubes are formed through etching along (001) direction [84]. Nanoflakes are formed by restraining the crystal growth along (001) direction using suitable precursor such as Zinc chloride [84]. Thus, different types of nanostructures can be obtained by controlling the growth along polar and non-polar surfaces for sensor application.

1.9 Chapter summary

In this section, history and classification of sensors are presented, starting from the general definitions, requirement of room temperature ammonia sensors, which constitute the main theme of this thesis. A part is related to the necessity and various applications of ammonia sensors and UV detector. A section of the chapter is focused on the semiconductor metal oxide sensors and importance of zinc oxide as sensing material. A section of the chapter is related to review on ZnO material. A brief description is presented on the growth mechanism of the different types of the nanostructures.

1.10 Objective and scope of the work

The main objectives of the work are to synthesize and characterize ZnO thin films and nanostructures (NS) for ammonia sensor and UV detection applications. The objectives of the work are summarized below:

1. For sensor applications, the growth of ZnO nanostructures on silicon substrates is highly preferred. In order to achieve well aligned ZnO NS, high quality seed layer of ZnO on Si substrate is required. In this section, thin layer of ZnO is deposited on silicon by RF sputtering technique and morphological evolution of sputtered ZnO thin films with variation in growth parameters are studied.

2. In order to enhance the crystallinity of the sputtered seed layer, post-deposition heat treatments (annealing) are carried out using rapid thermal annealing (RTA) system.

3. By adopting limited area heating, ZnO Ns are fabricated by using zinc nitrate and hexamethyltetramine (HMT) precursors. In this section, an attempt was made to grow various types of ZnO Ns (nanorods, nanowires, nanoplatelets) by modified aqueous method.

4. Ammonia sensing and UV detection behaviour of various types of ZnO thin films and nanostructures are measured under various conditions.

1.11 Organization of the thesis

The thesis aims to meet these above stated objectives. The complete work is proposed to be presented in six chapters including the introduction and conclusion.

Chapter 1

The first chapter is introductory, describing the necessity and importance of ammonia sensors. The current technology demands the miniaturizations of electronic devices, which can be possible by monolithic integration of sensors on silicon substrate. Although responsive and consistent NH_3 sensors have been fabricated based on ZnO nanostructures, they require high operating temperatures (typically > 250 °C) to trigger the adsorption and desorption processes of NH_3, which results in high power consumption and limits their use in low temperature applications. Thus, sensitive detection of NH_3 at room temperature is still highly required. This chapter also focuses on the importance of the zinc oxide as a promising material for ammonia sensor and UV detector. The types ZnO of nanostructure and their importance for sensor applications are also introduced.

Chapter 2

This chapter deals with the growth and characterization of the ZnO seed layer using RF magnetron reactive sputtering. A pure (99.99 %) metallic zinc target of 3 inch diameter and 0.25 inch in thickness was used as the zinc source. The sputtering parameters are optimized by

changing one of the four deposition parameters namely: sputtering power, substrate temperature, sputtering pressure, and Ar:O_2 ratio, while keeping other parameters unchanged.

Chapter 3

In this chapter, an investigation is carried out to study the effect of post-deposition annealing on sputtered ZnO seed layer. This study is imperative to know the microstructural changes that take place in the structural and morphological properties of ZnO seed layer with a view to grow well-aligned nanostructures. In order to grow nanostructures of various morphology for sensor applications; a good quality seed layer is highly essential. Rapid thermal annealing (RTA) at ZnO thin film with different temperatures, time and oxygen ambient is carried out. Co-relation between the morphological and the structural properties annealed ZnO seed layer is analyzed and discussed.

Chapter 4

This chapter emphasizes on growth of ZnO nanostructures arrays using limited area heating method. An investigation is carried out on various types of nanostructures (nanowires, nanorods, nanoplatelets, nanoflakes and network like porous structure). The chapter also reports on the change in morphology of nanostructures on addition of aluminum nitrate.

Chapter 5

In this section ammonia sensing and UV detection behaviour of ZnO thin film and nanostructures under various conditions was investigated. First part of the chapter mainly focuses on ammonia sensing of ZnO based on thin films and nanostructures at room temperature. In the second part, UV detection of various nanostructures is investigated. The main emphasis has been given to the transient photoresponse of nanostructures grown under different condition. The turn-off transients were fitted by using exponential equation. The decay time constant (τ) was calculated to investigate the relaxation time.

Chapter 6

The last chapter summarizes the work done in the thesis and highlights significant achievements. The thesis concludes with future scope of work.

1.12 References

[1] M. K. Sofian, M. E. Oussama, A. A. Imad, Sensors **9** 8158–8196 (2009).

[2] C. Wang, L. Yin, L. Zhang, D. Xiang, R. Gao, Sensors **10** 2088–2106 (2010).

[3] A. Wisitsoraat, E.T. Comini, W. S. Wlodarski, Thin Solid Films **517** 2775–2780 (2009).

[4] N. Yamazoe, K. Shimanoe, Sens. Actuators B **128** 566–573 (2002).

[5] X. Wang, J. Zhang, Z. Zhu, J. Zhu, Coll Surfaces A: Physicochem. Eng. Aspects **276** 59–64 (2006).

[6] J. Timmer, W. Olthuis, A. V. D. Berg, Sens. and Actuators B **107** 666–677 (2005).

[7] D. Kohl, J. Phys. D **34** 125–149 (2001).

[8] N. Docquier, S. Candel, a review Progr. Energy Combust. Sci. **28** 107–150 (2002).

[9] J. Riegel, H. Neumann, H.M. Wiedenmann, Solid State Ionics **153** 783–800 (2002).

[10] S. Ampuero, J.O. Bosset, Sens. Actuators B **94** 1–12 (2003).

[11] A. Dubbe, Sens. Actuators B **88** 138–148 (2003).

[12] D. N. Debarnot, F. P. Epaillard, Anal. Chim. Acta **475** 1–15 (2003).

[13] K. Zakrzewska, Thin Solid Films 391229–238 (2001).

[14] S.C. Chang, J.R. Stetter, C.S. Cha, Talanta **40** 461–477 (1993).

[15] I. Lundstrom, C. Sevensson, A. Spetz, H. Sundgren, F. Winquist, Sens. Actuators B **14** 16–23 (1993).

[16] T. Seiyama, A. Kato, Anal. Chem. **34** 1502–1503 (1962).

[17] W. H. Brattain, J. Bardeen, Bell Syst. Tech. J. **32** 1–41 (1952).

[18] Heiland, G. Zumeinfluss von wasserstoff auf die elektrischeleitfähigkeit von ZnO-kristallen. Z. Phys. **138** 459–464 (1954).

[19] P. J. Shaver, Appl. Phys. Lett. **11** 255–257 (1967).

[20] N. Taguchi, U.S. Patent 3 631 436 28 December 1971.

[21] C. S. Rout, M. Hegde, A. Govindaraj, C. Rao, Nanotechnology **18** 205504 (9) (2007).

[22] H. J Kim, J. H Lee, Sens. Actuators B Chem.**192** 607–627 (2014).

[23] K. Shimizu, I. Chinzei, H. Nishiyama, S. Kakimoto, S. Sugaya, W. Matsutani, Satsuma A. Sens. Actuators B, **141** 410–416 (2009).

[24] V. Srivastava and K. Jain Sens. Actuators B, **133** 46–52 (2008).

[25] N.G Deshpande, Y.G Gudage, Sharma R, J.C Vyas, J.B Kim, Y.P Lee. Sens. Actuators B **138** 76–84 (2009)

[26] K. Barrett, Atmos. Environ. **32** (3) 381–391(1998).

[27] J.W. Erisman, R. Otjes, A. Hensen, P. Jongejan, P. V. D. Bulk, A.Khlystov, H. Mols, Atmos. Environ. **35** 1913–1922 (2001).

[28] C. Pijolat, C. Pupier, M. Sauvan, G. Tournier, R. Lalauze, Sens. Actuators B **59** 195–202 (1999).

[29] G.H. Mount, B. Rumburg, J. Havig, B. Lamb, H. Westberg, D. Yonge, K. Johnson, **36** 1799–1810 (2002).

[30] D. J. Strike, M. G. H. Meijerink, H. Koudelka, Fres. J. Anal. Chem. **364** 499–505 (1999).

[31] C. Pijolat, C. Pupier, M. Sauvan, G. Tournier, R. Lalauze, Sens. Actuators B **59** 195–202 (1999).

[32] T.D. Durbin, R.D. Wilson, J.M. Norbeck, J.W. Miller, T. Huai, S. H. Environ. **36** 1475–1482 (2002).

[33] R. Moos, R. Muller, C. Plog, A. Knezevic, H. Leye, E. Irion, T. Braun, K.J. Marquardt, K. Binder, Sens. Actuators B **83** 181–189 (2002).

[34] P. Nag, Ph.d thesis, "Development of lead sulphide based gas sensor for ammonia detection", Department of instrumentation & electronics engineering faculty of engineering and technology Jadavpur University, Ch-1, p-9.

[35] X. J. Huang, Y. K. Choi, Sensors and Actuators B **122** 659–671 (2007).

[36] P. T. Moseley, Sensors and Actuators B **6** 149-156 (1992).

[37] D. R. Patil, L. A. Patil, Sensors and Transducers **70** 661-670 (2006).

[38] P. T. Moseley and D. E. Williams, Sensors and Actuators B **1** 113-115 (1990).

[39] W. Gopel, W. Reinhardt, Sensors Update **1** 49-120 (1996).

[40] E. Bekyarova, M. Davis, T. Burch, M. E. Itkis, B. Zhao, S. Sushine and R. C. Haddon J. Phys. Chem. B **108** 19717 (2004).

[41] A. Teeramongkonrasmee, M. Sriyudhsak, Sensors Actuators B **66** 256 (2000).

[42] Y. Wang, X. Wu, Q. Su, Y. Li, Z. Zhou, Solid-State Electron. **45** 347 (2001).

[43] P. Guo, H. Pan, Sensors Actuators B **114** 762 (2006).

[44] V. Romanovskaya, M. Ivanovskaya, P. Bogdanov, Sensors Actuators B **56** 31 (1999).

[45] E. Bekyarova, M. Davis, T. Burch, M. E. Itkis, B. Zhao, S. Sushine, R. C. Haddon, J. Phys. Chem. B **108** 19717 (2004).

[46] N. H. Quang, M. V. Trinh, B. Lee, J. Huh, Sensors Actuators B **113** 341 (2006).

[47] F. V. Paez, A. H. Romero, E. M. Sandoval, L. M. Martinez, H.Terrones, M.Terrones, Chem. Phys. Lett. **386** 137 (2004).

[48] C. S. Rout, S. H. Krishna, S. R. C. Vivekchand, A.Govindaraj, C. N. R. Rao, Chem. Phys. Lett. **418** 586 (2006).

[49] C. S. Rout, K. Ganesh, A. Govindaraj, C.N. R. Rao Appl. Phys. A **85** 241 (2006).

[50] C. S. Rout, A.Govindaraj, C. N. R. Rao, J. Mater. Chem.16 3936 (2006).

[51] A. Gurlo, N. Bârsan, U. Weimar, Chemistry and Applications; Fierro, J.L.G., Ed.; CRC Press: Boca Raton, FL, USA, 683 (2006).

[52] H. Nanto, T. Minami, S. Takata, J. Appl. Phys. **60** 482-484 (1986).

[53] P. T. Moseley, D. E. Williams, Sensors and Actuators B **1**.113-115 (1990).

[54] L. A. Patil, L. S. Sonawane, D. G. Patil, Journal of Modern Physics **2** 1215-1221 (2011).

[55] L.R. Narasimhan, W. Goodman, C. Kumar, N. Patel, Proceedings of the National Academy of Sciences **98** 4617-4621 (2001).

[56] C.Y. Lu, S. J. Chang, S.P. Chang, C.T. Lee, C. F. Kuo, H. M. Chang, P. Feng, T. H. Wang, Appl. Phys. Lett. **87** 213111 (2005).

[57] D. C. Kim, B.O. Jung, J. Lee, H. K. Cho1, J. Y. Lee, J. H. Lee, Nanotechnology **22** 265506 (2011).

[58] C.Y. Lu, S. P. Chang, S. J. Chang, T. J. Hsueh, C. L. Hsu, Y. Zung, Semicond. Sci. Technol. **24** 075005 (2009).

[59] S. Park, S. An, H. Ko, S. Lee, C. Lee, Sensors and Actuators B **188** 1270– 1276 (2013).

[60] J.G. Lu, P. Chang, Z. Fan, Mater.Sci.Eng. R 5249–91 (2006).

[61] A. R. Hutson, Phys. Rev. **108** 222-230 (1957).

[62] G. Heiland, E. Mollwo, F. Stockmann, Solid State Phys. **8** 193-196 (1959).

[63] J. R. Haynes, Phys. Rev. Lett. **17** 16 (1966).

[64] Y. S. Park, Phys. Rev. **143** 2 (1966).

[65] T. Damen, S. P. S Porto, B. Tell, Phys. Rev. **142** 2 (1966).

[66] Z. L. Wang, J. Phys. Condens. Matter **16** 829–858 (2004).

[67] O. Dulub, L. A. Boatner, U.Diebold, Surf. Sci. **519** 201 (2002).

[68] B. Meyer, D. Marx, Phys. Rev. B **67** 035403 (2003).

[69] P. W. Tasker, J. Phys. C: Solid State Phys. **12** 4977 (1979).

[70] O. Dulub, U. Diebold, G.Kresse, Phys. Rev. Lett. **90** 016102 (2003).

[71] A. Wander, F. Schedin, P. Steadman, A. Norris, R. McGrath, T. S. Turner, G. Thornton, N. M. Harrison, Phys. Rev. Lett. **86** 3811 (2001).

[72] V. Staemmler, K. Fink, B. Meyer, D. Marx, M. Kunat, S. G. Gil, U. Burghaus, C. Woll Phys. Rev. Lett. **90** 106102 (2003).

[73] Y. Ding, X. Y. Kong, Z. L. Wang, Phys. Rev. B **70** 235408 (2004).

[74] Z. R. Dai, Z. W. Pan, Z. L. Wang, Adv. Funct. Mater. **13** 9 (2003).

[75] M. H. Huang, Y. Y. Wu, H. Feick, N. Tran, E. Weber, P. D. Yang, Adv. Mater. **13** 113 (2001).

[76] R. S. Wagner, W. C. Ellis, Appl. Phys. Lett. **4** 89 (1964).

[77] C. Jagadish, S. J. Pearton, Thin Films and Nanostructures Processing, Properties and Application, Elsevier (2006).

[78] Z. L. Wang, Z. C. Kang, Plenum press **465** (1998).

[79] Z.L. Wang, J. Phys. Condensed Matter **16** 829 (2004).

[80] S. Lany, A. Zunger, Physical Review B. **72** 35215 (2005).

[81] Z. L. Wang, X. Y. Kong, Y. Ding, P. Gao, W. L. Hughes, R. Yang, and Y. Zhang, Adv. Funct. Mater. **14** 943 (2004).

[82] X. Y. Kong, Z. L. Wang, Nano. Lett. **3** 1625 (2003).

[83] X. Y. Kong, Y. Ding, R. Yang, and Z. L. Wang, Science **303** 1348 (2004).

[84] X. Y. Kong, and Z. L. Wang, Appl. Phys. Lett. **84** 975 (2004).

Chapter- 2

Growth of ZnO thin films by RF magnetron sputtering

2.1 Introduction

Now a days, transparent semiconducting zinc oxide (ZnO) thin films have drawn substantial interest because of its excellent properties like reflectivity in the infrared region, good chemical stability, UV absorption and high transparency in the visible region which makes ZnO well-suited for many optoelectronic and piezoelectric applications such as solar cells, flat displays, chemical and photosensors [1-2]. Basically, Zinc oxide is an n-type semiconductor with remarkable properties like its wide bandgap of ~3.37 eV at room temperature and high exciton binding energy (60 meV) [2-3]. In addition, ZnO is nontoxic and has strong tendency to grow along c-axis [2]. The versatile nature of ZnO makes it suitable for applications in number of solid-state electronic devices [1, 4-6]. In order to develop next generation of ZnO based portable, high performance, low power consumed robust nanoelectronic devices, well-aligned ZnO nanowires on CMOS compatible substrates are highly preferred. However, it is difficult to obtain well-aligned ZnO nanowires on bare Si substrates, because of the large differences in their thermal expansion coefficients and lattice mismatch [7]. Therefore, the implementation of a good quality seed layer with better morphological properties is an alternative process for the growth of well-aligned nanowires on Si substrate.

In current days, varieties of growth techniques are being implemented for deposition of thin films comprising of physical and chemical routes, such as pulsed laser deposition, thermal evaporation, chemical vapour deposition and magnetron sputtering [8-9]. Among these techniques, RF magnetron sputtering has several advantages such as its simplicity, low thermal budget allow use of flexible substrates, low-cost, nontoxic, and its ability to produce films of better quality [10]. The morphological properties of the seed layer depend greatly on growth parameters. In order to obtain high quality ZnO films, a systematic study on the variation of the sputtering parameters such as RF power, substrate temperature, working pressure and gas ratio are highly desired.

2.2 Experimental work

ZnO films were deposited on n-type silicon substrate [(100), 1-10 Ω.cm] using RF magnetron sputtering by varying RF powers from 75 W to 300 W and substrate temperature from room temperature to 300 ºC. A pure (99.99 %) metallic zinc target of 3 inch diameter was used as the zinc source. In order to generate the oxidation process of Zn, Ar/O_2 gas mixture was varied from 1:4 to 4:1 and the working pressure was varied from 4×10^{-3} mbar to 1×10^{-2} mbar during sputtering. The thickness of all the grown ZnO films was kept approximately 150 nm. The summary of deposition parameters of RF magnetron sputtering were mentioned in Table. 2.1.

Table. 2.1 Summary of deposition parameters of RF magnetron sputtering

RF Power (W)	Substrate temperature (°C)	Sputtering pressure ($\times10^{-3}$ mbar)	Gas flow ratio ($Ar:O_2$)
*VP1	200	4	2:3
150	*VP2	4	2:3
150	200	*VP3	2:3
150	200	4	*VP4
150	200	4	2:3

*Denotes varied parameters (VP)

VP1: RF Power (75 W, 150 W, 225 W, 300 W)

VP2: Substrate temperature (RT, 100 ºC, 200 ºC, 300 ºC,)

VP3: Sputtering pressure (4×10^{-3} mbar, 6×10^{-3} mbar, 8×10^{-3} mbar, 1×10^{-2} mbar)

VP4: Ar: O_2 gas flow ratio (1:4, 2:3, 3:2, 4:1)

2.2.1 Variation of RF power

Fig. 2.1 depicts the deposition rate of ZnO thin films grown on n-type (100) silicon substrate at different RF powers ranging from 75 W to 300 W. The deposition rate of the films was found to be increased with RF power. At higher sputtering power excess number of argon atoms became ionized to sputter higher amount of Zn and a result the film became thick.

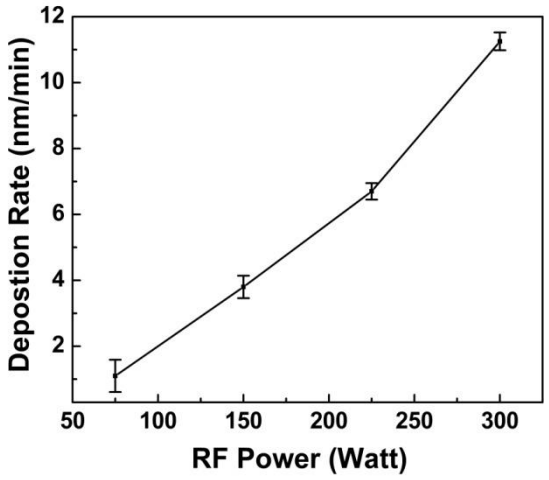

Fig. 2.1 Deposition rate of ZnO thin films with variation in RF power

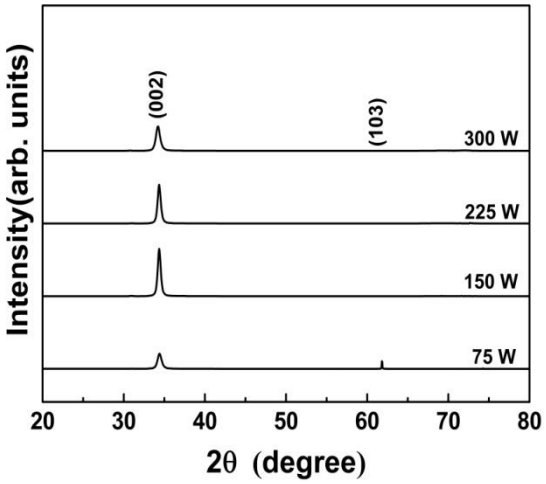

Fig. 2.2 X-ray diffraction patterns of ZnO thin films deposited at different sputtering powers ranging from 75 W to 300 W

Fig. 2.2 shows the XRD pattern of ZnO thin film deposited under different RF powers, where the substrate temperature is fixed at 200 ^{o}C. The results depicts that all the samples have c-axis preferred orientation with the evolution of a prominent (002) diffraction peak. At 75 W, an appearance of weak (103) peak of is observed, which disappeared at higher RF power. This corresponds to the phenomenon of "evolutionary selection" or "survival of the faster" [11-12]. As revealed above, it seems logical to conclude that increasing RF power promotes the growth of the preferred orientation (002) and hinders the growth of the other orientation. The films, grown at 150 W, have shown the highest degree of c-axis orientation. The (002) peak intensity was reduced for higher RF power (>150 W). This may be due to the faster sputtering as well as reaction rate of the zinc and oxygen species, where insufficient time is available for adatoms to be oriented along c-axis at the initial stage of deposition. Furthermore, the deterioration in the crystallinity at higher RF power may be due to the bombardment of excess energetic sputtered species on the substrate surface during the film growth.

Fig. 2.3 and Fig. 2.4 shows the FESEM images and surface roughness of ZnO thin films deposited with various RF power at a substrate temperature of 200 ^{o}C. FESEM images have shown uniform and continuous morphology of ZnO film. With the increase in RF power from 75 W to 300 W grains became smaller in diameter. It is believed that at higher RF power, the zinc atoms may have more chances to reach the substrates and increase the possibility of forming

nuclei. More nuclei existing on the substrate implies higher number of sites for grain growth. It means a large number of small grains can grow at the same time, which results smaller granular structure with smoother morphology.

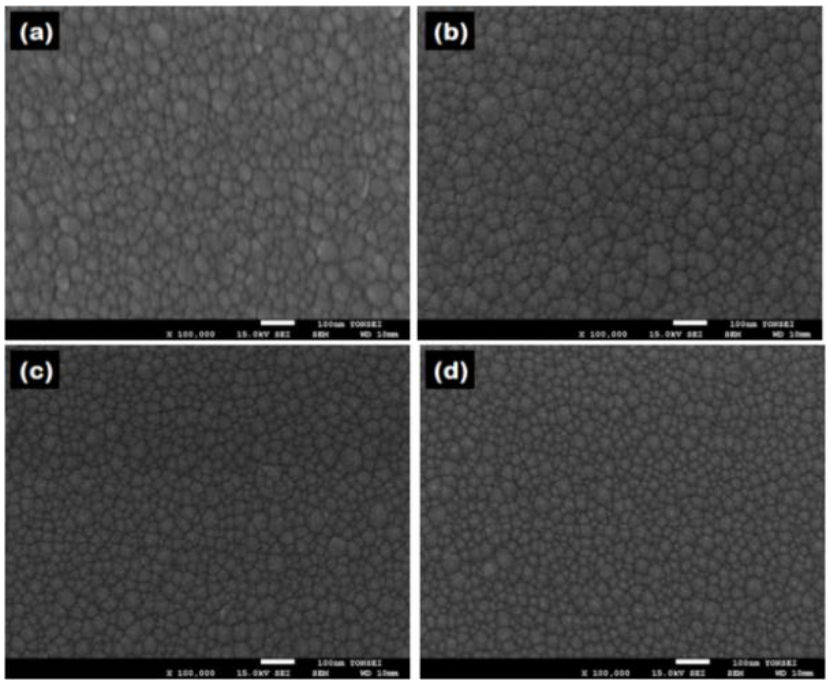

Fig. 2.3 FESEM images of ZnO thin film deposited on n-type silicon at (a) 75 W, (b) 150 W, (c) 225 W, and (d) 300 W. The scale bar represents 100 nm

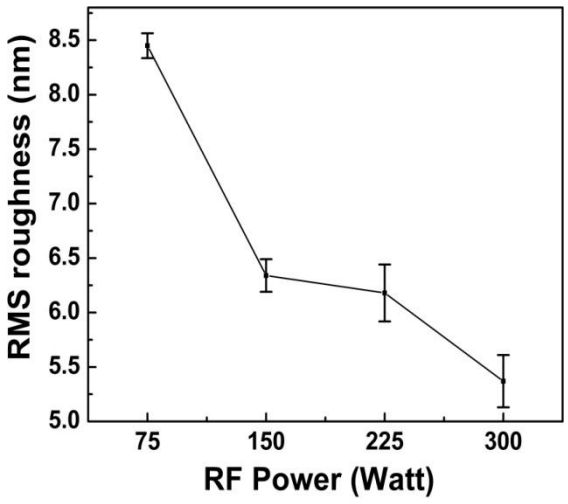

Fig. 2.4 Variation of RMS roughness as a function of RF power

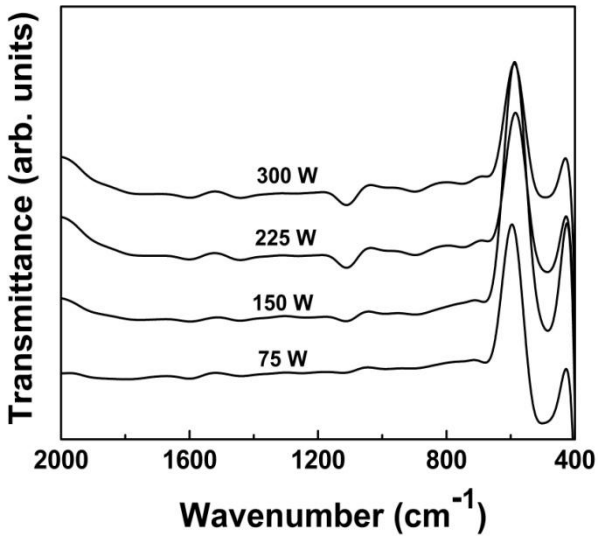

Fig. 2.5 FTIR transmittance spectra of ZnO thin films deposited at different RF powers

Fig. 2.5 shows the Fourier transform infrared (FTIR) transmission spectra of ZnO thin film deposited at different RF power ranging from 75 W to 300 W. The prominent absorption band is observed around 485 cm^{-1}, which is attributed to the characteristic Zn-O stretching bond. The band becomes prominent for the films deposited at 150 W indicating an increase in Zn-O bond density. For the RF power of 300 W, a slight shifting in the Zn-O peak is observed, which may be due to the change in morphology, because the position and number of absorption bands not only depends on crystal structure and chemical composition, but also on the morphology of deposited film [13]. In addition, the deviation of observed peak from its characteristic value might be due to the residual stress generated from the sputtering process. One additional bands centered at 1110 cm^{-1} corresponds to the Si-O stretching bond [13].

2.2.2 Variation of substrate temperature

Fig. 2.6 shows the variation in deposition rate of ZnO thin film with different growth temperature, where deposition rated decreases with increase in the substrate temperature. This may be due to the reduction of sticking coefficient by the increase in kinetic energy and mobility of adatoms at higher substrate temperature. On the other hand, the reduction of microvoids, pinholes may be one of the reasons behind the decrease in thickness.

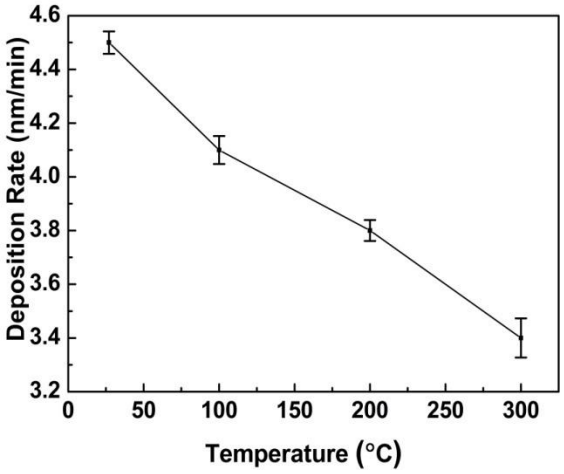

Fig. 2.6 Deposition rate of ZnO thin films with various substrate temperatures

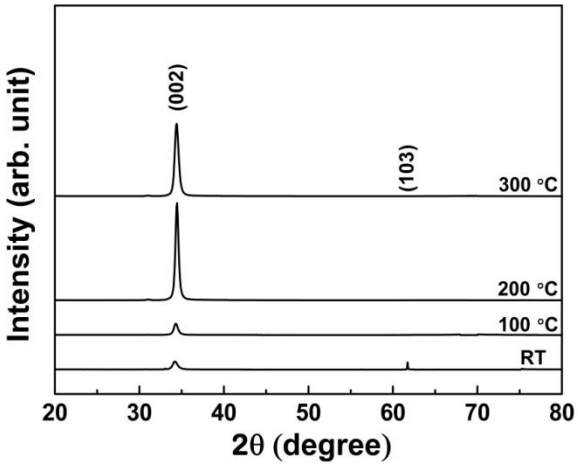

Fig. 2.7 X-ray diffraction patterns of ZnO thin films deposited at different substrate temperatures

Fig. 2.7 shows the XRD patterns of the ZnO thin film deposited at the optimized sputtering power of 150W with different growth temperatures starting from room temperature (RT) to 300 ^{o}C. The films are c-axis oriented with the appearance of (002) peak. The sample, grown at room temperature, shows one additional small peak (103) at 62^{o}. This peak was disappeared for the higher substrate temperature. The c-axis orientation in sputtered ZnO films is due to the lowest surface free energy of the (002) plane. The (002) peak becomes prominent at 200 ^{o}C, which depicts an improvement in the crystallinity of thin film. The decrease in crystallinity at higher temperature may be due to the presence of non-stoichiometric oxygen or incorporation of impurities during sputtering.

Fig. 2.8 shows the SEM micrographs of the ZnO films deposited at various substrate temperatures. The films deposited at room temperature shows smaller uniform grains. However, the films deposited at 300 ^{o}C have shown irregular shaped grains larger in size. Fig. 2.9 shows the increase in RMS roughness of ZnO films grown at different substrate temperature ranging from RT to 300 ^{o}C. This variation in morphology of the films with growth temperature may be due to the enhancement of surface mobility of the adatoms after arriving at the substrate surface at higher deposition temperature. Therefore, adatoms with higher mobility have tendency to migrate

towards the suitable lattice sites for successive growth. The particles, deposited at a low temperature, were not grown well due to the unavailability of excess thermal energy. The trend of variation of the RMS roughness with the substrate temperature is similar to the change of the surface morphology as depicted by FESEM images.

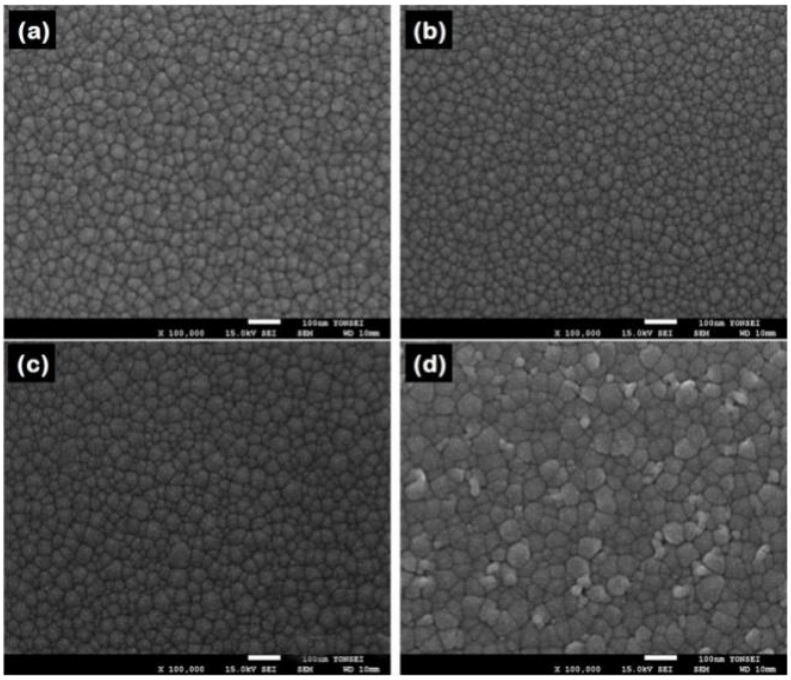

Fig. 2.8 FESEM image of ZnO thin film deposited on n-type silicon substrate at (a) RT, (b) 100 ^{o}C, (c) 200 ^{o}C, and (d) 300 ^{o}C. The scale bar represents 100 nm

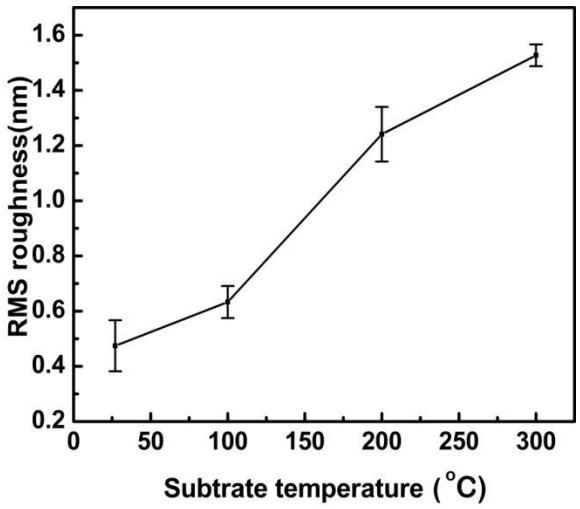

Fig. 2.9 Variation of RMS roughness at different substrate temperature ranging from RT to 300 ^{o}C

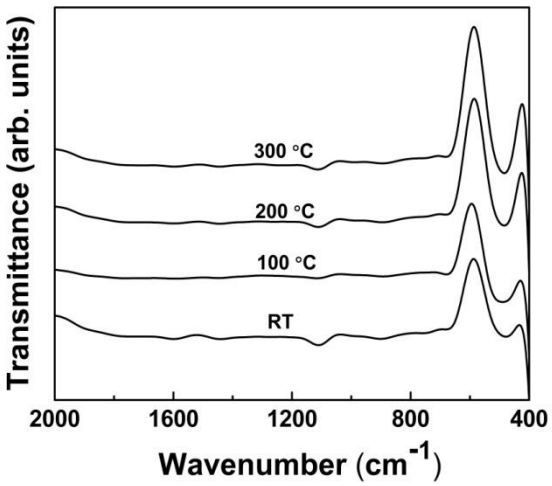

Fig. 2.10 FTIR transmittance spectra of ZnO thin films deposited at different substrate temperature ranging from RT to 300 ^{o}C

Fig. 2.10 shows the Fourier transform infrared (FTIR) spectroscopy transmission spectra of ZnO thin films deposited at different substrate temperatures. The absorption band around (485 cm^{-1}), is attributed to characteristic Zn-O stretching bond, which became prominent at higher deposition temperature. A small shift in this band is observed for at higher temperature, which may be due to the change in morphology and/or stress relaxation. The position and intensity of absorption bands not only depends on crystal structure and chemical composition, but also on the morphological arrangements of deposited film [13]. The peak appeared at 1110 cm^{-1} corresponds to the Si-O stretching bond.

2.2.3 Variation of working pressure

Fig. 2.11 depicts the dependence of pressure on the deposition rate of sputtered ZnO thin films. It has been observed that the deposition rate has higher value for low working pressure. It may be due to the longer mean free path of the sputtered species during low sputtering pressure, where the sputtered species follows directional motion with higher kinetic energy due to the less number of collisions. This enhancement of the kinetic energy promotes the arrival rate of adatoms on the substrate surface. On the other hand, the mean free path decreases at higher sputtering pressure due to the enormous collisions between particles resulting the frequent deviation in the directional motion as well as degradation of their momentum, which in fact decreases the growth rate.

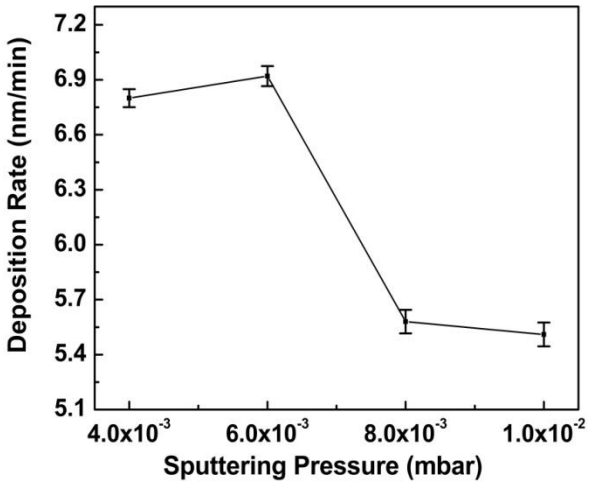

Fig. 2.11 Deposition rate of ZnO thin films at different sputtering pressure

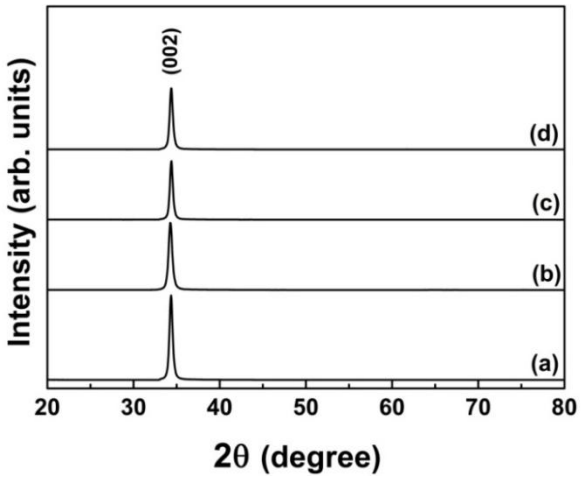

Fig. 2.12 XRD pattern of ZnO thin films deposited at different sputtering pressure (a) 4×10^{-3} mbar, (b) 6×10^{-3} mbar, (c) 8×10^{-3} mbar, and (d) 1×10^{-2} mbar

Fig. 2.12 shows the XRD pattern of ZnO thin film grown at different working pressures. Highly crystalline c-axis (002) oriented thin films are observed for lower sputtering pressure. During the growth process, the adatoms tend to orient in such a direction having minimum surface free energy. On the substrate surface, the adatoms migrate to the favorable growth direction only when they possess sufficient kinetic energy (high mobility). Therefore, the films deposited at lower sputtering pressure have shown relatively higher crystallinity. The deterioration in the crystallinity at higher sputtering pressure may be due to the loss of kinetic energy of the sputtered

species before reaching on the substrate surface.

Fig. 2.13 shows the FESEM images of the ZnO films grown at various sputtering pressures. The film deposited at lower working pressure has shown regular shape grains with uniform and homogeneous morphology. The grain size of the sputtered films found to be decreased with sputtering pressure. The films grown at the higher sputtering pressure consists of much larger grains and exhibits a rougher surface as compared to the film grown at lower pressure (Fig 2.14). This increase in RMS roughness may be due to the presence of grains of different shape and size as the sputtered species may have possessed a variation in kinetic energy as a result of random collisions at high sputtering pressure.

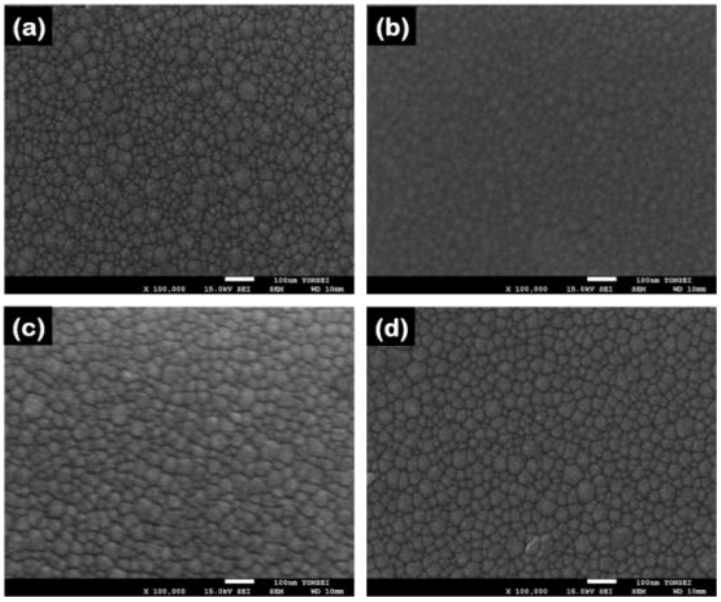

Fig. 2.13 FESEM images of ZnO thin films deposited at different sputtering pressure (a) 4×10^{-3} mbar (b) 6×10^{-3} mbar, (c) 8×10^{-3} mbar, and (d) 1×10^{-2} mbar. The scale bar represents 100 nm

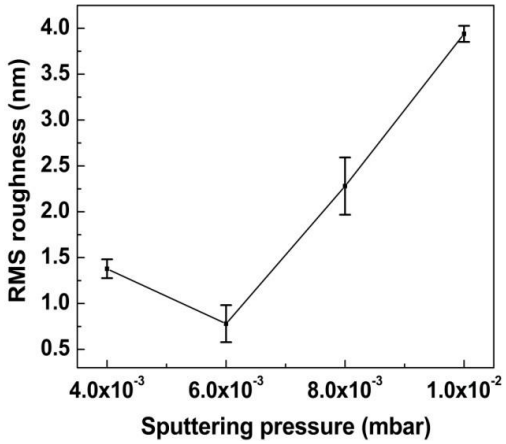

Fig. 2.14 Variation of RMS roughness as a function of different sputtering pressure

Fig. 2.15 shows the FTIR transmittance spectra of ZnO thin films deposited at different sputtering pressure ranging from 4×10^{-3} mbar to 1×10^{-2} mbar. FTIR spectrum is the characteristic feature of a particular compound providing information about its functional groups, molecular geometry and inter/intramolecular interactions. The prominent absorption band, observed around 485 cm^{-1}, is attributed to the Zn-O stretching mode, which became relatively prominent at lower pressure indicating the improvement in crystallinity as well as stoichiometry of the sputtered film. The peak observed at 1110 cm^{-1} corresponds to the stretching mode of Si-O bond [13].

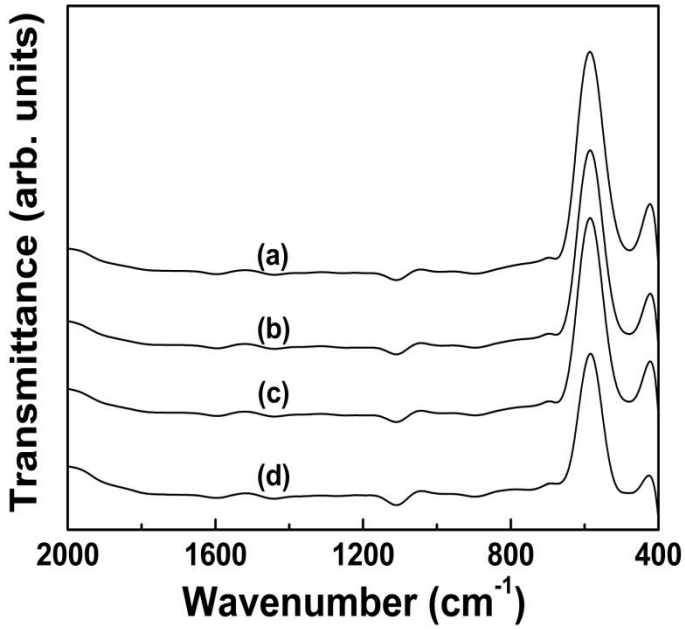

Fig. 2.15 FTIR transmittance spectra of ZnO thin films deposited at various sputtering pressure (a) 4×10^{-3}mbar, (b) 6×10^{-3}mbar, (c) 8×10^{-3}mbar, and (d) 1×10^{-2} mbar

2.2.4 Variation of Ar/O_2 gas flow ratio

Fig. 2.16 illustrates the deposition rate of the ZnO thin film as a function of Ar/O_2 gas flow ratio. It has been observed that the deposition rate decreases with the increase in oxygen concentration. This is attributed to the higher sputter yield of argon gas. As the ionization threshold of oxygen is higher than that of argon, the increase in oxygen concentration leads to weaker plasma and causes decay of deposition rate [14, 15].

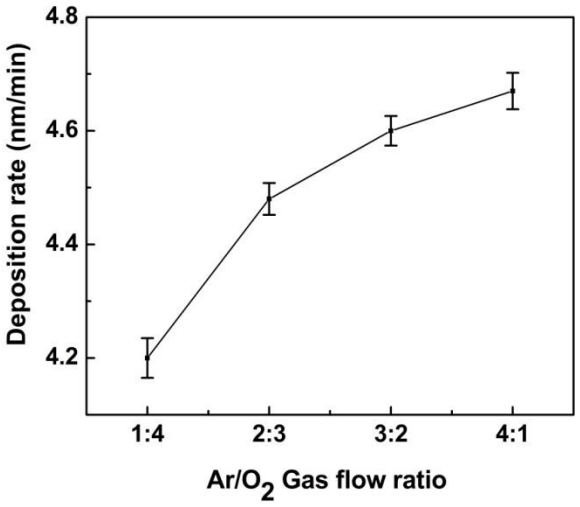

Fig. 2.16 Deposition rate of ZnO thin films deposited at different Ar/O_2 gas flow ratio

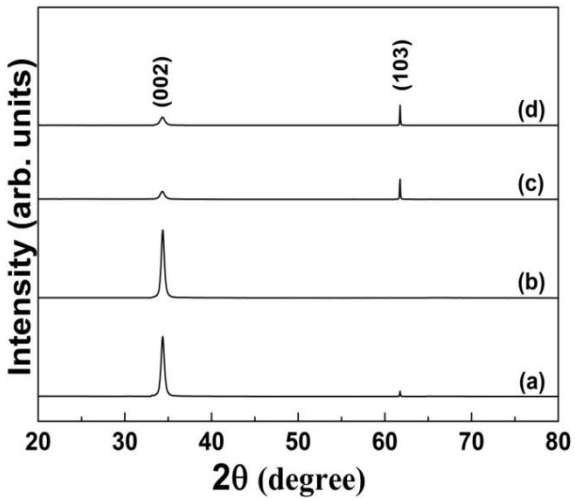

Fig. 2.17 XRD pattern of ZnO thin films deposited at different Ar/O_2 gas flow ratio. (a) 1:4, (b) 2:3, (c) 3:2, and (d) 4:1

Fig. 2.17 shows the XRD patterns of ZnO thin film deposited at different gas flow ratio. It is observed from the XRD spectra that all the deposited ZnO films exhibit a dominant peak corresponding to the (002) orientation at lower argon concentration. The films, grown at Ar/O_2 gas ratio of 2:3, has shown highest degree of crystallinity. In addition to c-axis orientation, a weak diffraction (103) peak is appeared at lower oxygen concentration. It has been reported that the crystallographic defects were increased at lower oxygen concentration, where stoichiometric deterioration taken place [16]. It has been observed that the relative intensity of (002) diffraction peak increases with an increase in oxygen concentration up to 60% and on further addition of oxygen the peak intensity decreases. This reduction in intensity may be due to the lower surface mobility of the adatoms and the accumulation of excess oxygen at the grain boundaries, which limits the growth of crystallites.

The surface morphologies of the ZnO films are investigated as a function of Ar/O_2 flow ratio by FESEM and AFM studies. Fig. 2.18 exhibits the FESEM of the ZnO films deposited at various Ar/O_2 gas flow ratios, where homogeneous distribution of granular structure is observed. The RMS roughness of the films, obtained from AFM studies, is plotted in fig. 2.19. Smoother surface is obtained at argon flow ratio of 2:3. The increase in surface roughness at higher argon concentration may be due to the high energetic ion bombardments.

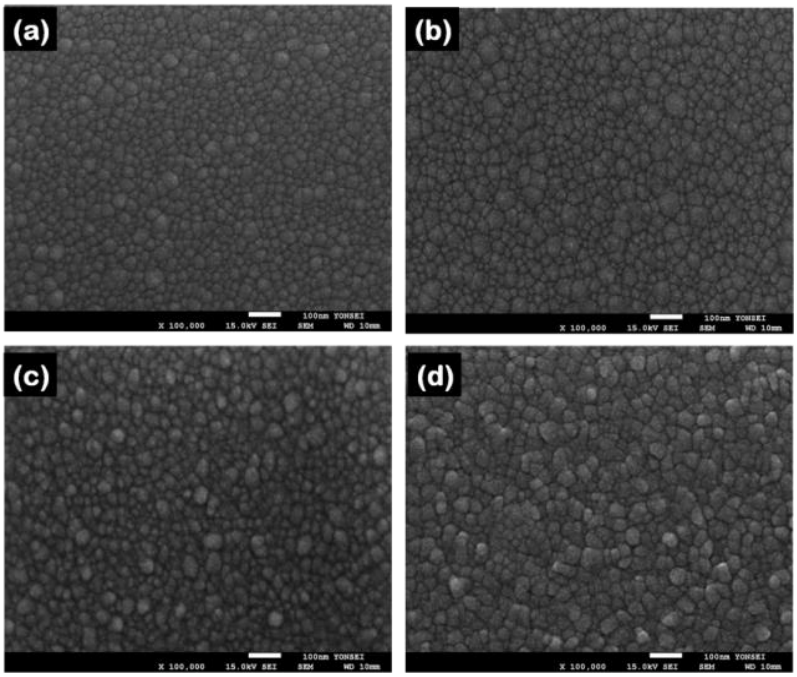

Fig. 2.18 FESEM image of ZnO thin film deposited at different Ar/O_2 gas flow ratio (a) 1:4, (b) 2:3, (c) 3:2, and (d) 4:1.The scale bar represents 100 nm

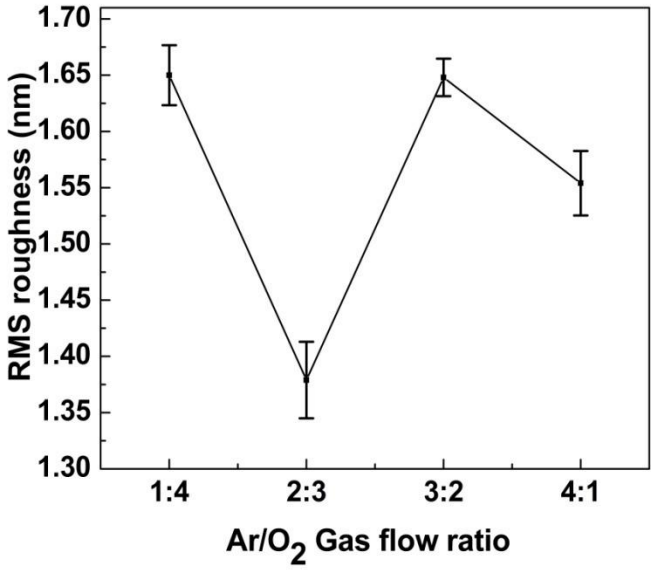

Fig. 2.19 Variation of RMS roughness as a function of different Ar/O_2 gas flow ratio

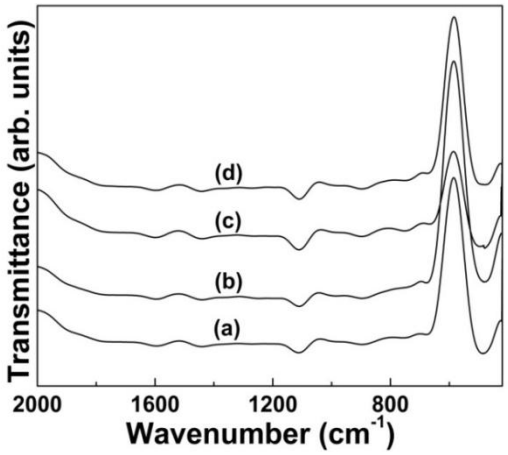

Fig. 2.20 FTIR transmittance spectra of ZnO thin films deposited at different Ar/O_2 gas flow ratio (a) 1:4, (b) 2:3, (c) 3:2, and (d) 4:1

Fig. 2.20 shows the Fourier transform infrared (FTIR) transmission spectra of ZnO thin film. The prominent peak, observed around 485 cm^{-1}, is attributed to the characteristic Zn-O bond. A relative broadening of this peak at higher argon concentration attributes to the deterioration of crystallinity as well as stoichiometry. This result agrees with the XRD observation. The peak, appeared at 1110 cm^{-1}, corresponds to the strecting mode of Si–O bond [13].

2.3 Chapter summary

ZnO thin films were deposited using sputtering technique by varying RF power and substrate temperature. The sputtered rate was greatly varied with the above parameters. C-axis oriented films were observed with the appearance of FTIR absorption peak at 485 cm^{-1}. The surface roughness and average grain size was found to be decreased with increase in RF power, where as films with bigger grains and higher roughness was observed at 300 ºC. The films, grown at the RF power of 150 W and substrate temperature of 200 ºC, found suitable for the use of seed layer. Further, highly crystalline c axis (002) oriented thin films are observed for lower sputtering pressure. The film deposited at lower working pressure has shown regular shape grains with uniform and homogeneous morphology. Investigation on variation of Ar/O_2 flow results in smoother surface at lower argon flow ratio concentration. The optimized pressure after investigation of various characterizations is found to be 4×10^{-3} mbar. Furthermore, $Ar:O_2$ gas flow ratio of 2:3 has shown highly crystalline c-axis oriented thin film.

2.4 References

[1] V. Senay, S. K. Pat, S. Balbag, Applied Surface Science **318** 2-5 (2014).

[2] A.Rosa, , E. d. Silva, M.Chaves, L. Trino, P. L. Filho, T. d. Silva, S. Durrant, J. Bortoleto, Journal of Material Science: Material Electron **24** 8 3143–3148 (2013).

[3] S. Takayanagi, T. Yanagitani, M. Matsukawa, Journal of Crystal Growth **363** 22-24 (2013).

[4] M. Yuste, G.R Escobar. R. Caretti, O. Sanchez, Journal of Physics D: Applied Physics **45** 025303 (2012).

[5] J. Tornow, K. Schwarzburg, Journal of Physical Chemistry C **111** 8692-8698 (2007).

[6] R.Zhang, S.Kumar, S. Zou, L. Kerr, Crystal Growth and Design **8** 381-383 (2008).

[7] J. P.Kar, S. Kim, B. Shin, J. M. Myong, J. M. Growth, Applied Surface Science Vol. **257** 4973–4977 (2011).

[8] W.C. Hsu, T. Cheng, W. Huang, J. Wu, C. Cheng, K. Cheng, S. Huang, Thin Solid Films **518** 1953–1957 (2010).

[9] W. Mtangi, F.D. Auret, J.V. Rensburg, P.J. Coelho, M.J. Legodi, J.M. Nel, W.E. Meyer, A. Chawanda, Journal of Applied Physics **110** 094504 (2011).

[10] J. P. Kar, S. Kim, B. Shin, J.M. Myong, Solid-State Electronics **54** 1447–1450 (2010).

[11] X.Yu, J. Ma, F. Jia, Y. Wang, X. Zhang, C. Cheng, M. Honglei, Journal of Crystal Growth **274** 474–479 (2005).

[12] K. Vijayalakshmi, K. Karthick, D. Gopalakrishna, Ceramics International **39** 4749–4756 (2013).

[13] Rajesh Das, Koel Adhikary, and Swati Ray Japanese Journal of Applied Physics **47** 3 1501–1506 (2008).

[14] Y. Igasaki and H. Kanma: Appl. Surf. Sci. **508** 169–170 (2001).

[15] Sang Sub Kim, Byung-Teak Lee, Thin Solid Films **446** 307–312 (2004).

[16] W. Lee, M.C. Jeong, J.M. Myoung, Acta Mater. **52** 3949 (2004).

Chapter- 3

Effect of rapid thermal annealing on RF sputtered ZnO thin films

3.1 Introduction

Zinc oxide (ZnO) thin films have engrossed considerable interest now a days, due to its excellent material properties like piezoelectricity, large bandgap semiconducting behaviour at room temperature [1-3]. Therefore, ZnO is currently used as multifunctional electronic material having applications in numerous areas such as light emitting diodes, laser diodes, varistors, piezoelectric transducers, field-effect transistors, touch display panels, flat panel displays, photovoltaic solar cells, and gas sensors and photodetectors due to its high chemical and high temperature stability, nontoxic nature and complementary metal oxide semiconductor (CMOS) compatibility [4-6]. Basically, the synthesis of high quality ZnO seed layer is mostly required for obtaining nanostructures of better quality. In current days, varieties of growth techniques are being implemented for deposition of thin films comprising of physical and chemical routes, such as pulsed laser deposition, thermal evaporation, chemical vapour deposition and magnetron sputtering [7-9]. Among these techniques, RF magnetron sputtering has several advantages such as its simplicity, low thermal budget allow use of flexible substrates, low-cost, nontoxic, and its ability to produce films of better quality with desired properties [10]. However, there is a chance of deterioration in the film quality due to the ionic bombardments or atomic intercollisions in the plasma during the sputtering, which generally gives rise to the formation of defects in the sputtered films. The electronic properties of the ZnO thin films are greatly influenced by these defect densities [3, 11-12]. Post-deposition heat treatments (annealing) are generally performed in order to annihilate the defects up to some extent [12]. Generally, annealing is broadly categorized into two types such as conventional furnace annealing (CFA) and rapid thermal annealing (RTA). RTA has several advantages such as low thermal budget, short processing time and less chance of dopant distribution [13]. Although few researchers have attempted to conduct post-deposition RTA process of ZnO thin films [13-16], a systematic study on the effect of RTA temperature, annealing time and oxygen flow rate on the physical properties of sputtered ZnO films has not yet been completely explored. In this section, the influence of RTA temperature, annealing time and oxygen flow rate on

the microstructural and optical properties of RF sputtered ZnO films are systematically investigated and correlated.

3.2 Experimental work

ZnO thin films were deposited onto n-type silicon [(100), 1-10 Ω.cm] substrates using reactive radio frequency (RF) magnetron sputtering technique at a constant substrate temperature of 200 °C. A pure (99.99 %) metallic zinc target of 3 inch diameter was used as the zinc source. In order to generate the oxidation process of Zn, Ar/O_2 gas mixture was supplied to the sputtering chamber during film growth. The plasma was activated at a RF power of 150 W with a sputtering pressure of 4×10^{-3} mbar. Thereafter, post-deposition RTA of the sputtered films was carried out by varying temperature (from 400 °C to 1000 °C), annealing time (from 150 seconds to 600 seconds) and oxygen flow rate (from 50 ml/min to 150 ml/min) using MTI (OTF 1200X) system.

3.2.1 Variation in annealing temperature

Fig. 3.1 shows the XRD pattern of ZnO films annealed at different RTA temperature ranging from 400 ^{o}C to 1000 ^{o}C in air ambient for 300 seconds. All the samples have shown c-axis orientation, where as a prominent (002) diffraction peak is observed for the sample annealed at 1000 ^{o}C. The gradual increase in peak intensity signifies a progressive improvement in the crystallinity along c-axis. Nonstoichiometric ZnO thin films are generally formed due to the presence of zinc interstitials or oxygen vacancies, which are responsible for the n-type conductivity in ZnO [17, 18]. During annealing, the atoms migrate to the favorable positions after receiving adequate amount of thermal energy in order to annihilate the defects and restructuring of the films take place along (002) orientation. The growth along c-axis is preferred due to its smallest surface free energy [19]. A shift in the (002) peak position towards higher diffraction angle attributes the stress relaxation due to the recrystallization and reduction of lattice imperfections of the annealed films in comparison to the as-deposited one [20].

Fig. 3.2 shows the FESEM images of ZnO thin film annealed at different RTA temperatures for 300 seconds in air ambient. Fig. 3.2 (a) depicts the granular surface morphology of as-deposited sample. The surface morphology is significantly modulated due to the evolution of bigger grains for the annealing temperature of 1000 ºC. In addition, structural modification is also observed with the appearance of small textures on the coalesced region.

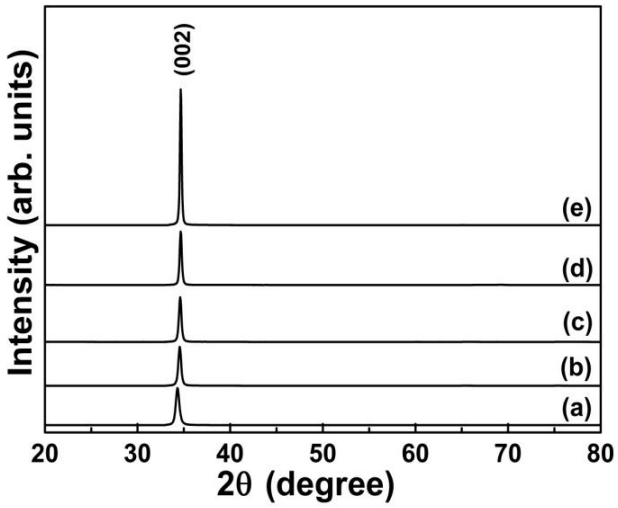

Fig. 3.1 X-ray diffraction patterns of ZnO thin films (a) as-deposited, and annealed at (b) 400 ^{o}C, (c) 600 °C, (d) 800 °C, and (e) 1000 °C in air ambient for 300 seconds

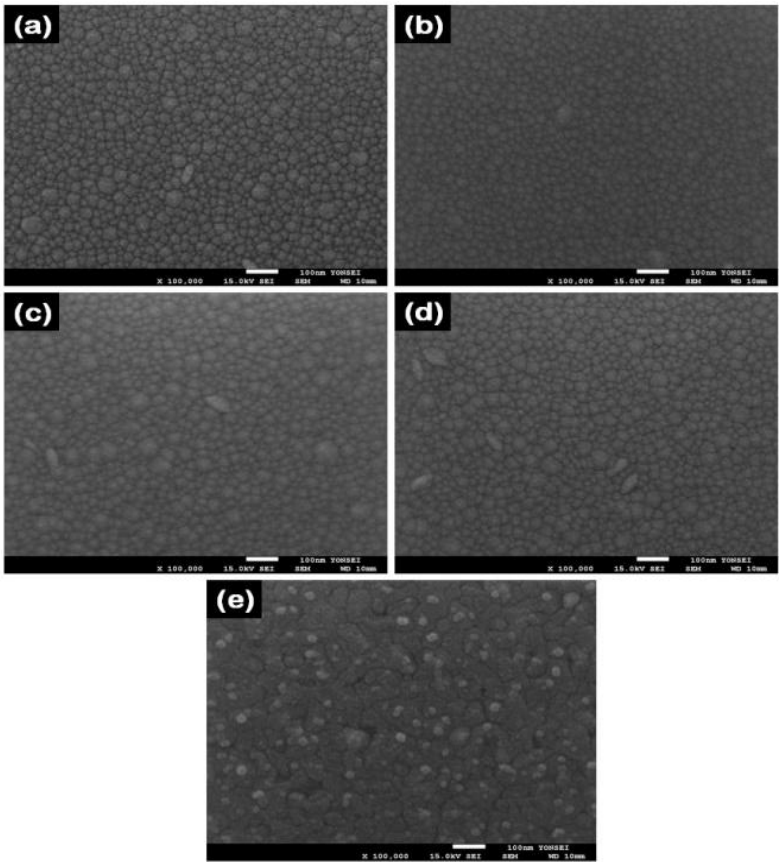

Fig. 3.2 FESEM images of ZnO thin films (a) as-deposited, and annealed at (b) 400 °C, (c) 600 °C, (d) 800 °C, and (e) 1000 °C in air ambient for 300 seconds. The scale bar represents 100 nm

Fig. 3.3 shows the evolution of surface roughness with the variation in the annealing temperature. A marginal increase in the roughness with the annealing temperature up to 800 °C is observed. The film, annealed at 1000 ºC, has shown higher surface roughness, which may be due to the evolution of larger grains as revealed by the SEM studies. The enhancement of the grain size at higher annealing temperature may be due to the relocation of grain boundaries by coalescence of smaller grains. This motion of grain boundary is due to atomic diffusion in grains when it received adequate amount of activation energy [21].

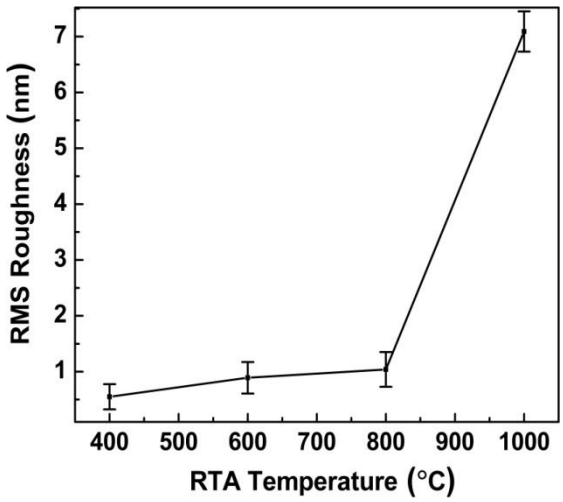

Fig. 3.3 Variation of RMS roughness of ZnO thin films annealed at various temperatures for 300 sec in air ambient

3.2.2 Variation in annealing time

Fig. 3.4 shows the XRD patterns of the ZnO thin films annealed at 1000 ^{o}C for a duration ranging from 150 seconds to 600 seconds in air ambient. All the samples exhibit a prominent (002) diffraction peak, which corresponds to the preferential orientation of the annealed films along c-axis. However, this peak intensity is deteriorated with annealing time, which may be due to the structural modification in the annealed films.

Fig. 3.5 shows the FESEM images of ZnO thin film annealed at 1000 ^{o}C in air ambient by varying process duration. It has been observed that the secondary grain growth became prominent with the increase in annealing duration. For annealing time of 150 seconds [Fig. 3.2(e)], newly generated smaller grains appeared on the coalesced bigger grain. This evolution of microstructures on the coalesced area became prominent with the increase in annealing time and as a result rough and porous surface is obtained. Longer annealing period provides sufficient time and thermal energy

to the ZnO microstructures for subsequent growth. This kind of restructuring of the grains may led to the formation of ZnO nanostructures, which is the scope of future research. Similar type of microstructural modulation has also been observed by Alvarado et al. [22]. The RMS roughness of the annealed films with various processing time is plotted in fig. 3.6, where the roughness of the ZnO films is found to be increased with annealing time. The FESEM and AFM analysis are well agreed with the XRD results.

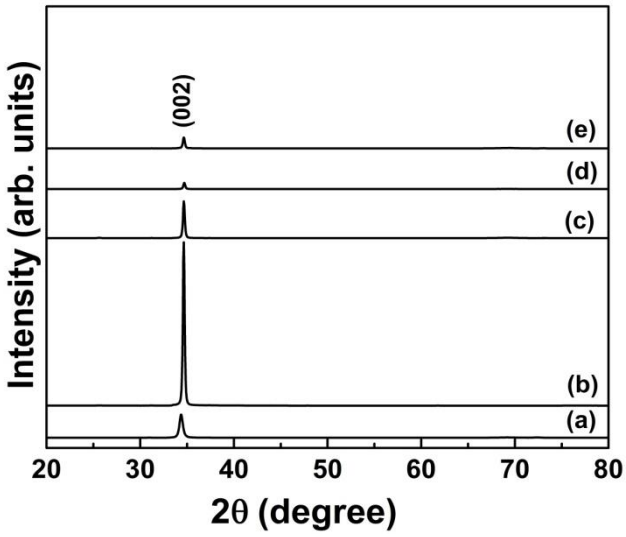

Fig. 3.4 X-ray diffraction patterns of ZnO thin films (a) as-deposited, and annealed at 1000 °C in air ambient for (b) 150 sec, (c) 300 sec, (d) 450 sec, and (e) 600 sec

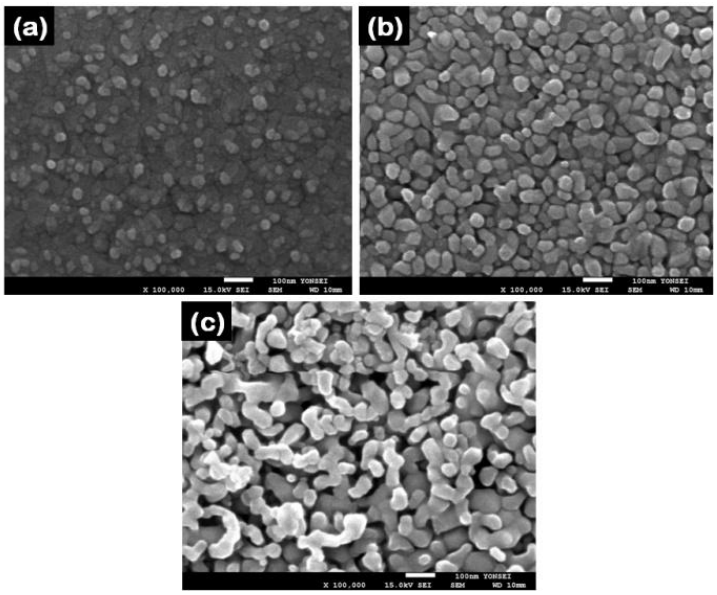

Fig. 3.5 FESEM images of ZnO thin films annealed at 1000 °C in air ambient for (a) 150 sec, (b) 450 sec, and (c) 600 sec. The scale bar represents 100 nm

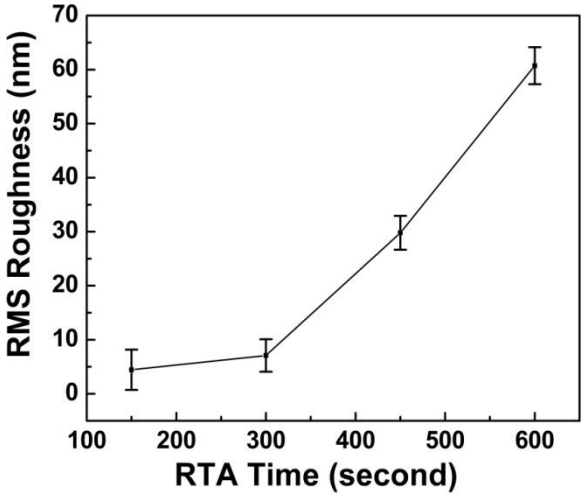

Fig. 3.6 Variation of RMS roughness of ZnO thin film annealed at 1000 °C in air ambient for various RTA duration

3.2.3 Annealing with different oxygen flow rate

Fig. 3.7 shows the XRD patterns of ZnO thin films annealed at 1000 °C for 150 seconds under different oxygen flow rate ranging from 50 ml/min to 150 ml/min. XRD plot of all the ZnO films exhibits a prominent (002) peak. The films, annealed at 150 ml/min, show higher degree of orientation in comparison to the flow rate of 50 ml/min. However, the films annealed in air ambient show better crystallinity.

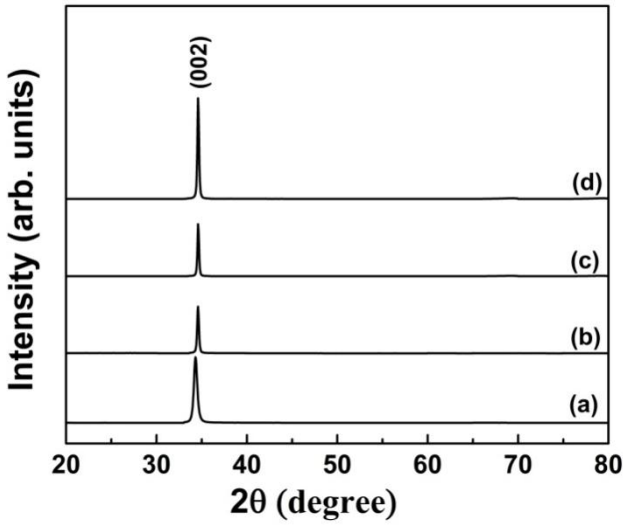

Fig. 3.7 X-ray diffraction patterns of ZnO thin films (a) as-deposited and annealed at 1000 °C for 150 sec with oxygen flow rate of (b) 50 ml/min, (c) 100 ml/min, and (d) 150 ml/min

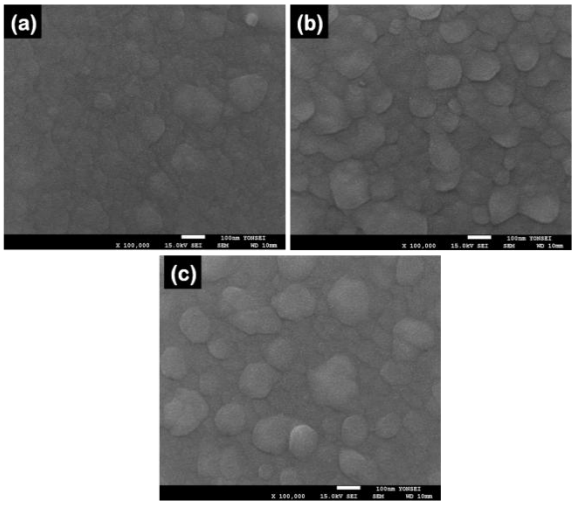

Fig. 3.8 FESEM images of ZnO thin films annealed at 1000 °C for 150 sec with oxygen flow rate of (a) 50 ml/min, (b) 100 ml/min, and (c) 150 ml/min. The scale bar represents 100 nm

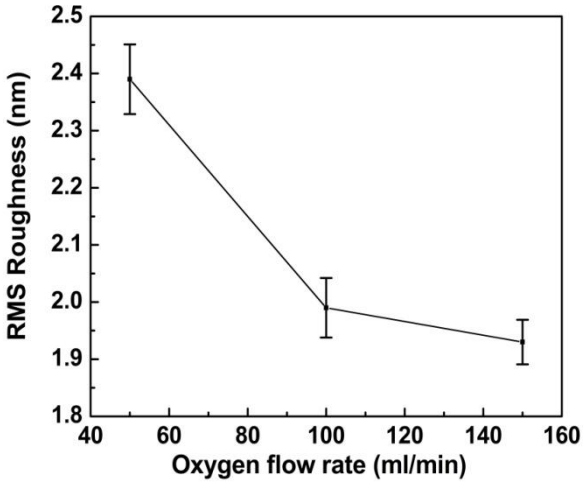

Fig. 3.9 Variation of RMS roughness of ZnO thin films annealed at 1000 °C for 150 sec with various oxygen flow rate

Fig. 3.8 depicts the FESEM images of the ZnO films annealed at 1000 ^{o}C for 150 seconds under various oxygen flow rate. Larger grains are formed due to the Ostwald ripening, where larger crystallites were grown by consuming the smaller adjacent crystallites during annealing in oxygen ambient. Fig. 3.9 shows the RMS roughness of the ZnO films with various oxygen flow rate during RTA process. The roughness of the film is found to be lowest for higher rate of oxygen flow due to the nonappearance of additional microstructures on its surface.

Fig. 3.10 shows the Fourier transform infrared (FTIR) transmission spectra of ZnO thin films annealed at 1000 °C for 150 seconds with various annealing ambient. A broad band centered at 485 cm^{-1} is attributed to characteristic absorption band of Zn-O stretching mode [23-25]. As a result of annealing, the band becomes prominent, indicating an increase in Zn-O bond density. This increase in Zn-O bond network may be due to the diffusion of oxygen into the film during RTA process, which greatly depends on the annealing temperature and its ambient. In polycrystalline films, grain boundaries may act as channels for rapid incorporation of oxygen inside the film, which in fact enhances the microscopic rearrangement of Zn–O bond network through oxidation of Zn atoms. This band became prominent as a result of annealing, which could be associated with the improvement in the ZnO crystallinity. One more additional band centered at 1110 cm^{-1} corresponds to the Si-O stretching bond [25].

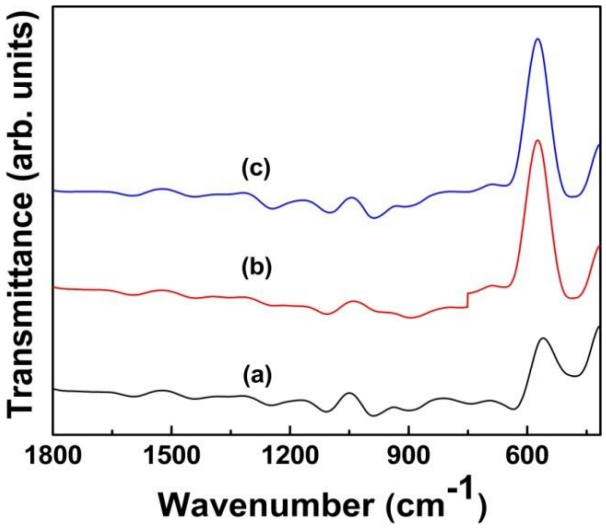

Fig. 3.10 FTIR transmittance spectra of ZnO thin films (a) as-deposited, and annealed at 1000 °C for 150 sec (b) in air ambient, and (c) with O_2 flow rate of 150 ml/min

3.3 Chapter summary

RF sputtered ZnO thin films were subjected to rapid thermal annealing with varying annealing parameters such as temperature, annealing duration and ambient. Relatively high c-axis (002) oriented films were obtained at 1000 °C in air ambient for an annealing duration of 150 seconds. The surface of the films, annealed for 600 seconds, became rough due to the evolution porous microstructures, whereas the films annealed in oxygen ambient has shown smoother surface morphology. The characteristic absorption band of Zn-O became prominent due to the increase in Zn-O bond density by the oxidation of unbounded zinc atoms during the RTA process.

3.4 References

[1] B.C. Mohanty, B.K. Kim, D.H. Yeon, Y.H. Jo, I. J. Choi, S.M. Lee, and Y.S. Cho, J. Electrochem. Soc. **159** H96-H101 (2012).

[2] C. Wang, D. Xu, X. Xiao, J. Mater. Sci. **42** 9795-9800 (2007).

[3] U. Ozgur, Ya. I. Alivov, C. Liu, A. Teke, M. A. Reshchikov, S. Dogan, V. Avrutin, S.J. Cho, and H. Morkoc J. Appl. Phys. **98** 041301 (2005).

[4] A. Radzimska and T. Jesionowski, Materials **7** 2833-2881 (2014).

[5] J. Mou, W. Zhang, J. Fan, H. Deng and W. Chen, Journal of Alloys and Compounds **509** 961–965 (2011).

[6] J. Loureiro, S. Filonovich, Frederic W. Neves, R. Barros, S. Reparaz, L. Divay, T. Mateus, C. Torres, R. Martins, R. Santos, and I. Ferreira, J. Mater. Chem. A **2** 6649 (2014).

[7] C. W. Hsu, T. Cheng, W. Huang, J. Wu, C. Cheng, K. Cheng, and S. Huang, Thin Solid Films, **518** 8 1953–1957 (2010).

[8] W. Mtangi, F. D. Auret, J. Rensburg, P.J. Coelho, S.M. Legodi, M.J. Nel, J.M. Meyer, A. Chawanda, Journal of Applied Physics **110** 9 094504 (2011).

[9] C. Periasamy, R.Prakash, P. Chakrabarti, J Mater Sci: Mater Electron **5** 9912 (2009).

[10] J. P Kar, S. Kim, B. Shin and J. M. Myoung, SolidState Electronics **54** 1447–1450 (2010).

[11] K.C. Sekhar, S. Levichev, K. Kamakshi, S. Doyle, A. Chahboun, M.J.M. Gomes, Materials Letters **98** 149–152 (2013).

[12] G.P. Daniel, V.B. Justinvictor, P.B. Nair, K. Joy, P. Koshy, P.V. Thomas, Physica B **405** 1782–1786 (2010).

[13] J. Li, J.H.Huang ,Y.Zhang ,Y. Yang ,W. Song, X.M. Li, J. Electroceram. **26** 84–89 (2011).

[14] Y. Lee, S.Hu, W. Water, Y.S. Huang, M. D. Yang, J. Shen, K. K. Tiong, C. Huang, Solid State Communications **143** 250–254 (2007).

[15] N. A. Suvorova, I. O. Usov, L. Stan, R. F. Paula, A. M. Dattelbaum, Q. X. Jia, A. A. Suvorova, Applied Physics Letters **92** 141911 (2008).

[16] W. Cheong, M. Ryu, J. Shin, S. Park, C. Hwang, Thin Solid Films **516** 8159–8164 (2008).

[17] A.K Srivastava and J. Kumar, Sci. Technol. Adv. Mater. **14** 065002 (2013).

[18] A. Janotti and CG Van de Walle, Rep. Prog. Phys. **72** 126501(2009).

[19] P.T. Hsieh, Y.C. Chen, C.M. Wang, Y.Z. Tsai, C.C. Hu, Appl. Phys. A, Material Science and Processing **84** 345–349 (2006).

[20] G. Anil Kumar, M.V.R. Reddy, K.N. Reddy, Journal of Physics: Conference Series **365** 012031 (2012).

[21] Z.W. Liu, W.J. Fu, M. Liu, J.F. Gu, C.Y. Ma, Q.Y. Zhang, Surface and Coatings Technology **202** 5410-5415 (2008).

[22] J.A. Alvarado, A. Maldonado, H. Juarez, M. Pacio, R. Perez, Beilstein J. Nanotechnol. **6** 971–975 (2015).

[23] S.Y. Hu, Y.C. Lee, J.W. Lee, J.C. Huang, J.L. Shen, W. Water, Appl. Surf. Sci. **254** 1578–1582 (2008).

[24] Y.C. Lee, S.Y. Hu, W. Water, K. Tiong, Z.C. Feng, T. Chen, J. C. Huang, J. W. Lee, C. Huang, J.L. Shen, M.H Cheng, Journal of Luminescence **129** 148–152 (2009).

[25] K.Vijayalakshmi, K. Karthick, D. Gopalakrishna, Ceramics International **39** 4749–4756 (2013).

Chapter- 4

Growth of ZnO nanostructures by modified aqueous chemical method

4.1 Introduction

Zinc oxide (ZnO) possesses a rich family of nanostructures (nanowires, nanorods, nanoflakes, nanotubes etc.) and has their realistic applications for future next generation of electronic devices. The inspiration behind the development of low dimensional nanostructures (NS) with superior sensing behaviour is its enhanced surface area. Therefore, extensive research on the growth of low dimension ZnO with various surface morphology is very essential. Since the performance of the sensors strongly depends on the morphology of ZnO NS, it is very essential to specifically control their orientation and surface morphology to exploit its properties in different realistic fields. In order to obtain ZnO NS with high aspect ratio and well-aligned orientation, many vacuum related techniques have been devoted such as vapor–liquid–solid (VLS) and metal organic chemical vapor deposition (MOCVD) method [1-3]. However, these methods have some drawbacks such as expensive apparatus, complicated procedure and high temperature operation. Thus, there is a need of simple robust technique for the growth of various types of ZnO NS. Hydrothermal and electrochemical processes are two important low temperature approaches for the growth of ZnO NS [4-7]. Hydrothermal method was first introduced by Vaysseries et al. for the growth of ZnO nanowires [8]. The main advantages of low-temperature solution routes over other methods are their simplicity, low cost and large-area production [9]. In order to develop next generation of reliable and high performance sensors, vertically aligned ZnO NS on CMOS compatible silicon substrates are highly preferred. However, due to large lattice mismatch and difference in thermal expansion coefficient, it is difficult to obtain vertically aligned ZnO nanostructures on bare silicon substrates [10-12]. Therefore, the implementation of a highly crystalline seed layer with better morphological properties is an alternative approach for the growth of vertically aligned ZnO NS on Si substrate. In this chapter, the growth of various types of ZnO NS, on seed layer coated silicon substrates by limited area heating method, is discussed.

4.2 Modified aqueous chemical growth method

One of the problems associated with the hydrothermal synthesis of the ZnO NS is the ramp up and ramp down temperature, which spanned from several minutes to hours. In case of global heating of the solution, the reaction can't be processed for longer duration due to unavailability of fresh precursors. In order to overcome this problem, an attempt has been made by slight modification of the aqueous method by limited area heating. The schematic layout of limited area heating system is shown in fig. 4.1. Unlike conventional global heated aqueous chemical growth (ACG), limited area heating method has several advantages such as fast ramp up or ramp down, low thermal budget, precise control over growth temperature and growth duration. This modified aqueous chemical growth method has ability to produce uniform and homogeneous array of NS. In this method, the formation of nuclei in the bulk solution is reduced due to residence time of the reactants in the heated zone is less. Therefore, this method may produce nanowires of high aspect ratios for a process of longer period.

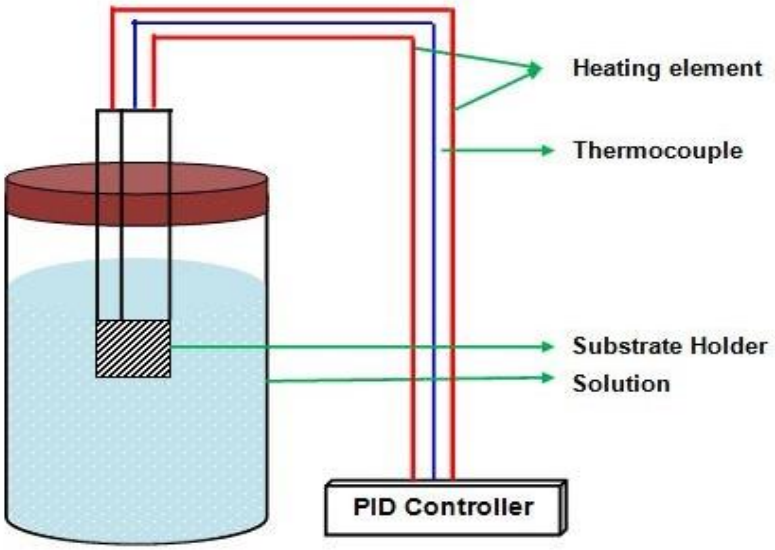

Fig. 4.1 The schematic layout of limited area heating system

The reaction takes place only near the heated substrate and therefore there is very less chance of production of undesired NS in the other parts of the reaction chamber. Due to the limitation on the undesired growth, this method has ability to produce different NS without adding any additional chemicals during the entire process. This strategy consumes only a little

amount of reactants during growth i.e. most of the chemicals remain in the cold part of the solution for subsequent long period growth. This technique has abilities to (i) produce homogeneous NS, (ii) reduce contamination by avoiding the formation of unwanted long nanorods in the bulk of solution. The morphology of the NS can be varied by a precise control over the process parameters. This approach of synthesis may provide a suitable platform to several semiconductors in order to develop and co-integration of next generation of composite, embedded, hybrid low-dimensional electronics devices and sensors.

Precursors play a vital role in hydrothermal process, because the whole growth mechanism is reaction dependent and is ruled by the chemistry laws. It has been reported that ZnO NS can be synthesized using different zinc salts such as zinc nitrate hexahydrate, zinc chloride and zinc acetate dihydrate by hydrothermal method [3, 13-14]. The most successful and well reproducible growth of ZnO NS is the hydrolysis of zinc nitrate in water in the presence of hexamethyltetramine (HMT) [15-16]. During the growth process of NS via hydrothermal route, zinc nitrate basically provides Zn^{2+} ions. On the other hand, HMT is a non-ionic cyclic tertiary amine which act as a bidentate Lewis base that coordinates and bridges two Zn^{2+}ions [17-18]. In the reaction, HMT decomposes to give ammonia, which plays two essential roles for the growth of ZnO NS. Primarily, it creates basic environment required for the formation of zinc hydroxide. Secondly, it coordinates with Zn^{2+} ions and stabilizes aqueous Zn^{2+} ions. The following chemical reactions are governing the growth process [19-22].

$$HMT + 6\ H_2O \leftrightarrow 4\ NH_3 + 6\ HCHO$$

$$NH_3 + H_2O \leftrightarrow NH_4^+ + OH^-$$

$$Zn^{2+} + 2\ OH^- \leftrightarrow Zn(OH)_2$$

$$Zn(OH)_2 \leftrightarrow ZnO + H_2O$$

4.3 Experimental work

In this work, silicon substrates were used to grow ZnO NS by modified aqueous method. Before the growth process, pieces of silicon with a surface 1.5×1.5 cm^2 were ultrasonically cleaned by successive treatment of acetone, isopropanol and deionized (DI) water from Milli-Q system (~18.3 MΩ-cm) for 10 min each followed by acid treatment. A seed layer of ZnO (200 nm) was deposited onto n-type silicon [(100), 1-10 Ω.cm] substrates using reactive radio frequency (RF) magnetron sputtering technique at 200 °C. A pure (99.99 %) metallic zinc target of 3 inch diameter was used as the zinc source. In order to generate the oxidation process of Zn, Ar/O_2 gas mixture was supplied to the sputtering chamber during film growth. The plasma was activated at a RF power of 150 W with a sputtering pressure of 4×10^{-3} mbar. The films were subjected to post deposition rapid thermal annealing process in order to enhance the crystallinity.

In order to grow ZnO NS, hydrothermal solution was prepared by mixing equimolar aqueous solutions of the zinc nitrate $Zn(NO_3)_2$ (purity > 99%) and HMT (purity 99 %). All chemicals were purchased from Sigma Aldrich and used without further purification. The substrate coated with the seed layer was mounted on the substrate holder and the whole system was then immersed in the specific volume of the prepared solution. The substrate is then heated to the desired temperature by a heater, which is placed inner side of the substrate holder. The reactions are processed for duration of 5 hours. At the end of the growth process, substrates were taken out of the solution, rinsed with DI water to remove residual salts and organic material and finally dried at room temperature.

4.3.1 Growth of ZnO nanowires/nanorods

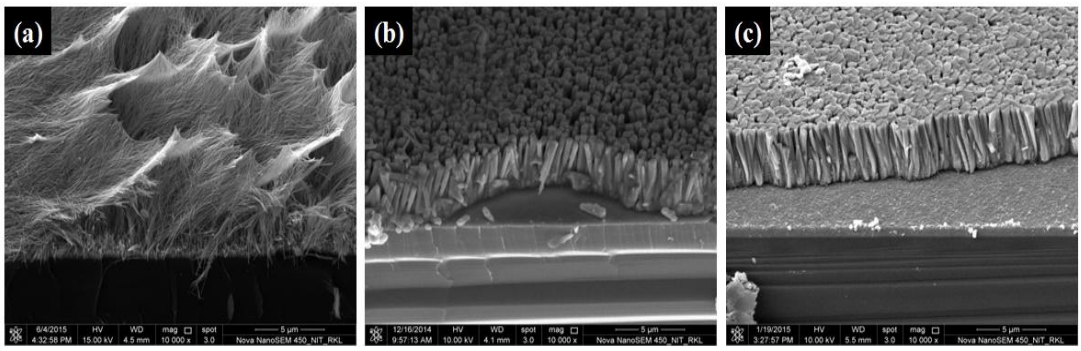

Fig. 4.2 FESEM images of ZnO nanostructures grown at 95 ^oC (a) 0.01M, (b) 0.025M, and (c) 0.05M. The scale bar represents 5µm

Fig. 4.2 depicts the tilted cross-sectional FESEM images of ZnO nanostructure grown at 95 °C in an equimolar solution of Zinc nitrate hexahydrate and HMT with different concentrations of 0.01 M, 0.025 M, and 0.05 M. The effect of concentrations on the diameters and lengths of ZnO NS were observed. The samples grown at lower concentration (0.01 M) results in thin and long nanowires with a diameter < 30 nm, and the length was found to be around 5-6 µm, [Fig. 4.2(a)]. A nanorod-like morphology was observed at a solution concentration of 0.025 M with an average diameter around 150 nm and length of 3-5 µm [Fig. 4.2(b)]. Further increase in the concentration of 0.05 M, vertical aligned thick nanorods (diameter: 600–1000 nm, length: 3-5 µm) were appeared [Fig. 4.2(c)]. With an increase in solution concentration, a significant increase in the nanowire diameter was observed along with a decrement in length. This change in dimension with higher concentration may be due to the availability of more ionic species in the growth solution. At higher concentration, more number of closely spaced nuclei is formed at the initial stage. Afterwards, some of newly grown thin NS merge together to form thicker nanorods during the subsequent growth.

Fig. 4.3 depicts the crystalline nature of hydrothermally grown ZnO NS with the appearance of (002) peak. Besides, additional peaks along the plane (100), (101) and (103) planes are also observed. No characteristic peaks of other impurities were detected in the pattern.

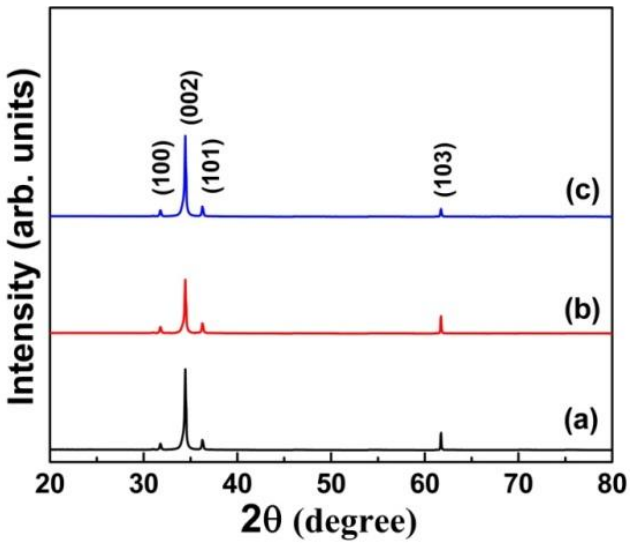

Fig. 4.3 X-ray diffraction pattern of ZnO nanostructures grown at 95 ^{o}C (a) 0.01 M, (b) 0.025 M, and (c) 0.05 M

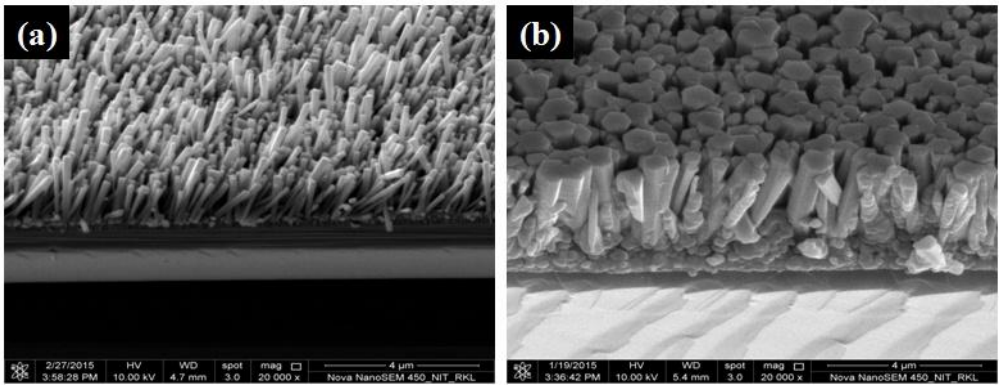

Fig. 4.4 FESEM images of ZnO nanostructures grown (a) 0.01 M at 85 °C, and (b) 0.05 M at 75 ^{o}C. The scale bar represents 4 µm

As the growth of ZnO nanostructures is a thermo-activated process, the temperature greatly stimulates the nano structure morphology. Short ZnO nanorods (length: 2-3 µm, diameter: 350-410 nm) were obtained, when growth process was conducted at 85 °C. Although low temperature favours the formation of nucleation sites, it does not have enough energy for the subsequent growth of NS. At higher concentration (0.05 M) with growth temperature of 75 ^{o}C, short and stubby NS are obtained (Fig. 4.4). It indicates that the growth temperature is not sufficient for faster growth along c-axis and therefore, the length of NS was restricted.

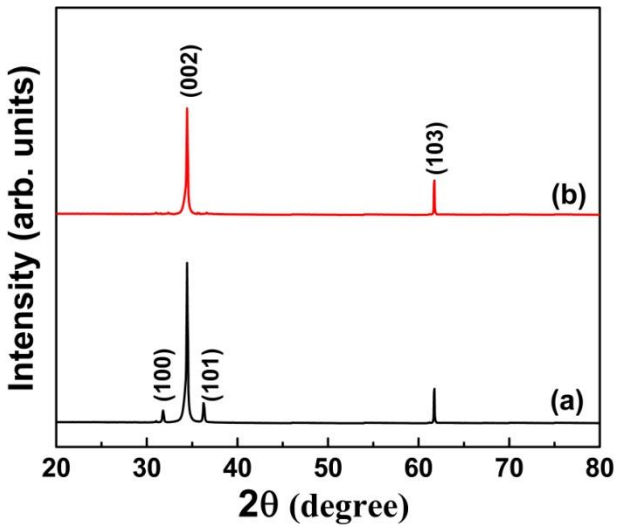

Fig. 4.5 X-ray diffraction pattern of ZnO nanostructures grown (a) 0.01 M at 85 °C, and (b) 0.05 M at 75 ^{o}C

Fig. 4.5 shows the X-ray diffraction pattern of the grown ZnO NS. A prominent (002) orientation along with small (103) peaks were observed for all the samples, which depicts the growth of NS along c-axis. ZnO peaks in the spectrum affirmed that the obtained products have good crystallinity. Two additional (100), (101) peaks has been observed for the sample grown at 0.01 M. No characteristic peaks of other impurities were detected.

4.3.2 Growth of ZnO nanoplatelets/nanoflakes

As the growth of nanostructures follows bottom up technique, the addition of small amount of specific chemicals have the ability to change the morphology of nanostructures due to the formation of additional chemical complexes, which generally restricts the c-axis growth [23-25]. Thus, an attempt has been done by the addition of appropriate amount of aluminum nitrate with $Zn(NO_3)_2$ and HMT precursor. In order to investigate the effect of aluminium, aluminium nitrate nonahydrate [$Al(NO_3)_3.9H_2O$, 99.997 % Sigma Aldrich] powders were added according to 1-5 at.% of aluminium in equimolar solution of $Zn(NO_3)_2$ and HMT. The hydrothermal process was carried out in modified aqueous system at 95 ^oC.

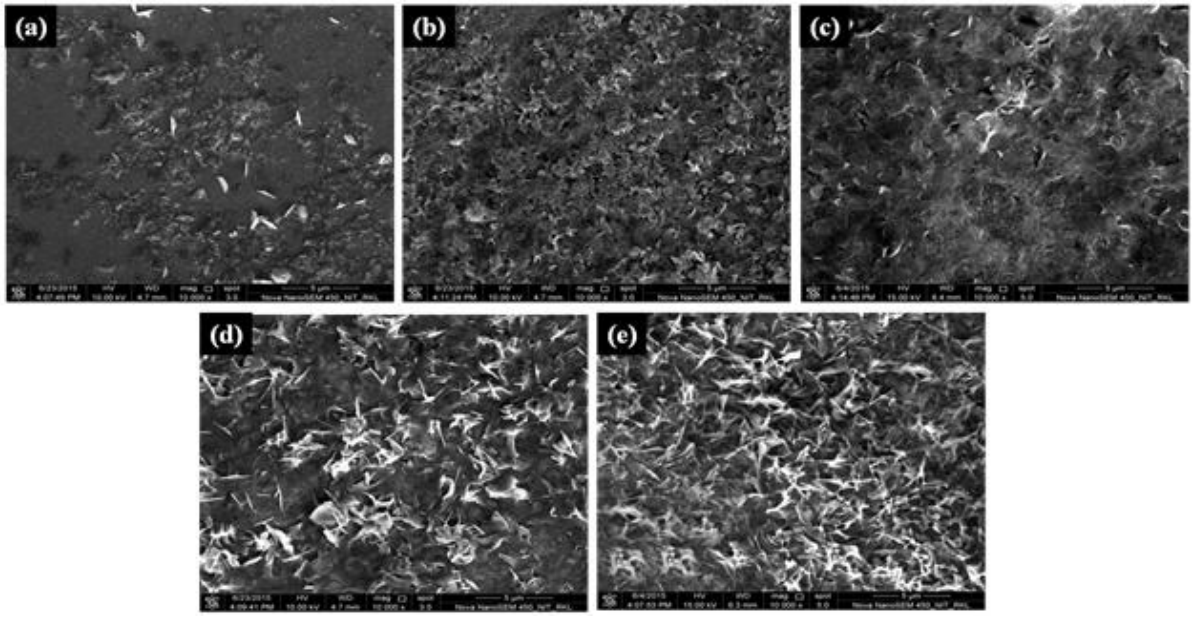

Fig. 4.6 FESEM images of ZnO nanostructures with addition of (a) 1 at.%, (b) 2 at.%, (c) 3 at.%, (d) 4 at.%, and (e) 5 at.% aluminium. The scale bar represents 5 µm

It is clearly evident from the FESEM micrograph (Fig. 4.6) that the ultrathin flake-like nanostructures have grown on seed layer. FESEM images depicts the formation of non-uniform flakes like structures having width around 400-600 nm. In this study, the change in morphology of nanostructures has been observed due to the presence of Al species [25]. These Al-complexes bind to the polar surfaces and the growth of ZnO NS along c-axis is restricted. As a result, growth of ZnO NS along lateral direction takes place, which in fact gives rise to the formation of ZnO nanoflakes/platelets.

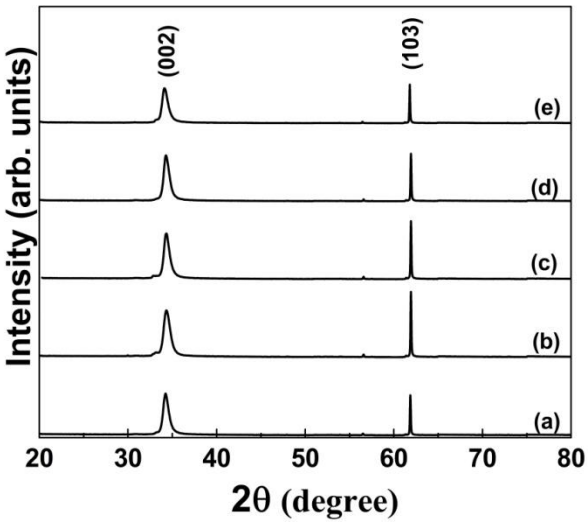

Fig. 4.7 X-ray diffraction pattern of nanostructure with addition of (a) 1 at.%, (b) 2 at.%, (c) 3 at.%, (d) 4 at.%, and (e) 5 at.% aluminum

Fig. 4.7 shows the XRD patterns of the nanostructures with the addition of aluminum nitrate. Two peaks along the (002) plane and (103) has been observed, which confirms the formation of ZnO phase. No other characteristic peaks corresponding to the impurities were detected in the XRD patterns.

4.3.3 Growth of ZnO network like porous structure

Fig. 4.8 shows the FESEM images of ZnO NS grown by modified aqueous method. In order to investigate the growth of NS at lower temperature, external water circulation was given during the growth. The concentration of the solution was kept at 0.025 M and the reaction was carried out at 65 ^{o}C for 5 hours duration. It has been observed that porous and dense

interconnected network like structures are formed uniformly enveloping the whole substrate. The width of the interlinked strips was varied between 50-120 nm, whereas the pore has wide variation in diameter. The formation large porous network like area is may be due to the lateral growth of those interlinked strips. However, exact mechanism behind this type of network like porous structure can be studied by investigating different stages of the growth, which is the scope of future research. Fig. 4.9 represents the X-ray diffraction pattern of hydrothermally grown ZnO network like porous structure. Intense c-axis oriented (002) peak is observed shows higher crystallinity of porous structure.

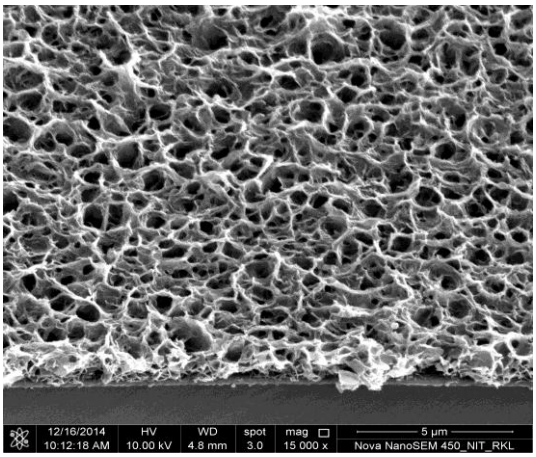

Fig. 4.8 FESEM image of hydrothermally obtained network like porous structure of ZnO. The scale bar represents 5µm

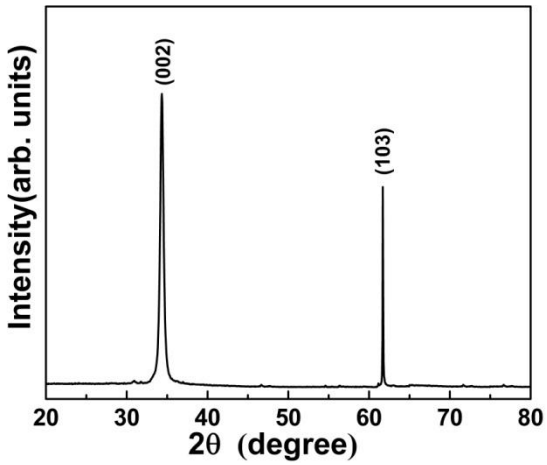

Fig. 4.9 XRD pattern of hydrothermally grown network like porous structure of ZnO

4.4 Chapter summary

This chapter emphasizes on growth of oriented ZnO nanowires/nanorods arrays using limited area heating method. In order to obtain vertically aligned nanostructures on silicon substrate, ZnO film is used as a seed layer. It has been observed that the morphology of the ZnO nanostructures is significantly influenced by the variation in growth conditions of the aqueous method. Thin nanowires are obtained at growth temperature of 95 °C for 0.01 M concentration, whereas thick nanorods are found at 75 °C for 0.05 M concentration. ZnO nanoplatelets/ nanoflakes like structure are formed on adding specific amount of aluminium nitrate nonahydrate

in the above precursors. In addition, network like porous structure were obtained as a result of low temperature growth.

4.5 References

[1] R. Wahab, Y.S. Kim, H. S. Shin, Materials Transactions **50** 2092- 2097 (2009).

[2] M.H. Huang, S. Mao, H. Feick, H. Yan, Y. Wu, H. Kind, E. Weber, R.Russo, P. Yang, Science **292** 1897 (2001).

[3] M. C. Akgun, Y. E. Kalay, H. E. Unalan, J. Mater. Res. **27**, 1445-1451 (2012).

[4] L. E. Greene, B. D. Yuhas, M. Law, D. Zitoun, P. Yang, Inorg. Chem. **45** 7535-7543 (2006).

[5] C. C. César,M. C. Gnambodoe, Y. L. Wang, Appl. Phys. A **115** 953–960(2014)

[6] J.X. Wang, X.W.S, Y. Yang, H. Huang, Y.C. Lee, O.K. Tan, Nanotechnology **17** 4995 (2006)

[7] J. Wang, L. Gao, Solid State Commun. **132** 269 (2004).

[8] L. Vayssieres, Adv. Mater. **15** 464 (2003).

[9] M. Guo, P. Diao, S. Cai, J. Solid State Chem. **178** 1864 (2005).

[10] J. P. Kar, S. Kim, B. Shin, J. M. Myoung, Solid-State Electronic **54** 11 (2010).

[11] K.C. Sekhar, S. Levichev, K. Kamakshi, S. Doyle, A. Chahboun, M. J. M. Gomes, Materials Letters **98** 149–152 (2013).

[12] J. Cui, Materials characterization **64** 43– 52 (2012).

[13] S. F. Wang, T. Y. Tseng, Y. R. Wang, C. Y. Wang, H. C. Lu, W. L. Shih, Int. J. Appl. Ceram. Technol. **5** 419 (2008).

[14] J. Elias, R. T. Zaera, C. L. Clément, J. Electroanal. Chem. **621** 171 (2008).

[15] H. E. Unalan, P. Hiralal, N. Rupesinghe, S. Dalal, W.I. Milne, G.A.J. Amaratunga, Nanotechnology **19** 255608 (2008).

[16] S. W. Chung, J.Y. Yu, J. R. Health, Appl. Phys. Lett. **76** 2068–2070 (2000).

[17] I. S. Ahuja, C. L. Yadava, R. J. Singh, Mol. Struct., **81** 229–234 (1982).

[18] S. Baruah, J. Dutta, Sci. Technol. Adv. Mater. **10** 013001 (2009).

[19] M.H. Mamat et. al., Japanese Journal of Applied Physics **50** 06GH04 (2011).

[20] J. P. Kar, S. Kim, B. Shin, J. M. Myoung, Applied Surface Science **257** 11 (2011).

[21] C. W. Hsu, T. Cheng, W. Huang, J. Wu, C. Cheng, K. Cheng, S. Huang,Thin Solid Films **518** 8 (2010).

[22] S. Xu, Z. L.Wang,Nano Res. **4** 1013–1098 (2011).

[23] Y. Jia, X.Y. Yu, T. Luo, M. Y. Zhang, J. H. Liu, X. J. Huang, Cryst. Eng. Comm. **15** (2013) 3647.

[24] T. Wang, Y. Liu, G. Li, Z. Sun, J. Lu ,B. Liu, M. Wu, Cryst. Eng. Comm **13** 2661 (2011).

[25] X. Fan, G. Fang, S. Guo, N. Liu, H. Gao, P. Qin, S. Li, H. Long, Q. Zheng, X. Zhao, Nanoscale Research Letters **6** 546 **(**2011).

Chapter- 5

Ammonia sensing and UV detection behaviour of ZnO thin films and nanostructures

5.1 Introduction

Sensitivity of a material is mainly dependent on the surface area of the sensing material, which enhances the interaction between the materials and its surrounding environment. Among numerous chemicals, detection of ammonia is vital due to its toxic and extensive use in many areas, such as environmental monitoring, fertilizer and chemical industries [1]. Different types of semiconducting metal oxide materials, conducting polymers are used for ammonia detection [2]. However, polymers are thermally unstable and moisture sensitive, which limits their high temperature application [3]. On other hand, metal oxide semiconductor such as ZnO based NH_3 sensors require high operating temperatures (typically > 250 °C) to trigger the adsorption and desorption processes of NH_3, which results in consumption of high power and limits their use in low temperature applications [4-6]. Thus, sensitive detection of ammonia at room temperature is still highly required.

In recent years, UV light is used in many commercial fields such as telecommunications, ozone and pollution monitoring, high temperature flame detection, and missile warning systems [1–3]. The well-established CMOS compatibility semiconductor such as silicon (Si) has some limitation for UV detection due to its low bandgap (1.1 eV). Since the bandgap energy of Si is 1.1 eV, costly high pass optical filters and phosphors are needed to stop low energy photons [7-9]. Therefore, the Si based UV detector performance will be significantly reduced by lowering the efficiency and increase of dark currents [10-11]. However, the bandgap of ZnO (3.37 eV) corresponds to the intermediate region between UV and visible light. In addition, outstanding physical and chemical properties of ZnO nanostructures (NS) such as large surface area, radiation hardness [12], superior spatial resolution [13] and high electron mobility provide a platform for versatile applications for UV detection.

5.2 Ammonia sensing characteristics of ZnO thin films and nanostructures

The sensing action of ZnO thin films depends on several factors such as surface area and surface states as well as the efficiency with which the sensing material molecules adsorb as well as desorb on the surface [1, 14]. Ammonia sensing mechanism is generally explained in terms of variation in resistance either by adsorption of oxygen from atmosphere or by direct interaction of lattice oxygen or interstitial oxygen with ammonia. The overall ammonia response at room temperature is based on surface adsorption process. The sensing mechanism of ZnO (intrinsic n-type) involves the formation of depletion layer on the surface due to trapping of electrons by adsorbed oxygen species (O_2^-, O_2^{2-}) present on the surface [15-16]. The ammonia sensing mechanism is given by:

$$O_2(\text{ads.}) + 2\,e^- \rightarrow 2\,O^-(\text{ads.})$$
$$2\,NH_3 + 3\,O^-(\text{ads.}) \rightarrow 3\,H_2O + N_2 + 3\,e^- \qquad (1)$$

After interacting with ammonia these adsorbed oxygen releases the trapped electron back to the conduction band of ZnO in order to enhance the conductivity by reducing the width of the depletion layer [17-18].

5.2.1 Experimental work

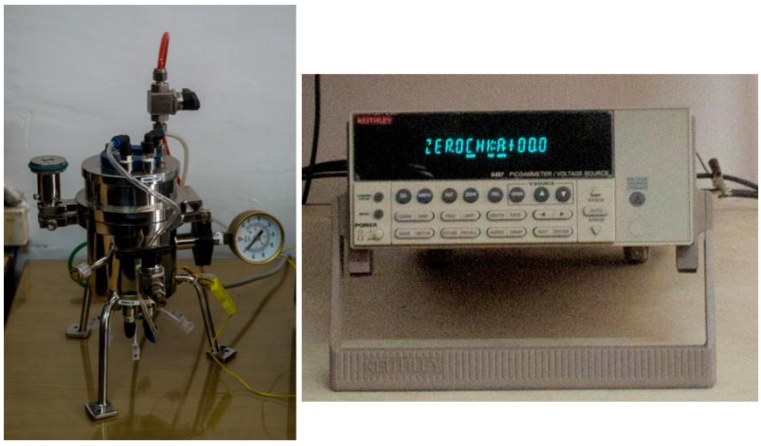

Fig. 5.1 Custom-designed gas sensing chamber and Keithley 6487 picoammeter/voltage source

For NH_3 sensitivity measurement, ZnO based sensors were prepared by deposition of seed layer using RF sputtering technique followed by growth of nanostructure by modified aqueous chemical method. Top electrodes were deposited by thermal evaporation of aluminum at high vacuum (5×10^{-6} mbar) by adopting shadow mask techniques. Gas sensing properties were measured using a custom-designed computer-controlled characterization system consisting of a test chamber, sample holder, a Keithley 6487 Picoammeter/Voltage source as shown in the Fig. 5.1. For monitoring the response of the films to ammonia gas, the samples were mounted in 1000 cc air tight testing chamber. All the gas sensitivity measurements were carried out at room temperature. The current flowing through the samples was measured using a Keithley 6487 Picoammeter/Voltage source. By calculating the change in sample resistance, the sensitivity was estimated. It can be expressed as

$$\text{Sensitivity (\%)} = \frac{\Delta R}{R}\times 100 \qquad (2)$$

Where ΔR is the change in resistance of the sensor due to presence of ammonia and R is the original resistance sensor in air. In addition to sensitivity, response time and recovery time of a sensor are also two important characteristics.

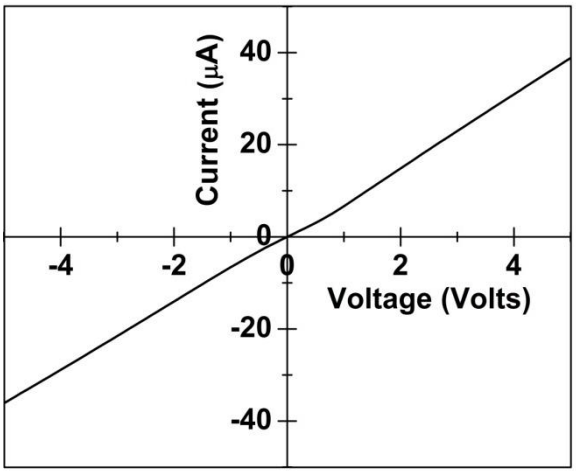

Fig. 5.2 Current -voltage plot of ZnO thin film based sensor/detector in air ambient

Before measuring the ammonia sensitivity and UV detection, the Ohmic contact of the samples has been observed by taking the current-voltage measurement. Linear enhancement of

current with sweep in voltage of ±5V for all samples depicted good Ohmic nature of the electrical contact. Fig. 5.2 represents the current voltage characteristic of ZnO thin film based sensor/detector before sensing. The details of the samples used for sensing application, are given in Table. 5.1.

Table. 5.1 Comparative study of ammonia sensing and UV detection behaviour of various samples

Sample No.	**Sample Type**	**Growth Condition**	**Ammonia Sensitivity (%) at 1000 ppm**	**UV on/off ratio**	**Decay Constant (τ in sec.)**
S1	ZnO thin film	150 W, 200 ^{o}C, 4×10^{-3} mbar, Ar/O_2-2:3	6.1	1.5	47
S2	Annealed film	1000 ^{o}C, 600 sec	8.2	1.7	21
S3	Nanowires	95 ^{o}C, 0.01M	46.3	6.1	39
S4	Nanorods	75 ^{o}C, 0.05M	16.9	2.9	57
S5	Nanoplatelets	95 ^{o}C, 0.01M, Al 3%	29.4	5.3	84
S6	Nanoflakes	95 ^{o}C, 0.01M, Al 5%	8.5	5.2	44
S7	Network like porous structure	65 ^{o}C, 0.025M (with external cooling)	73.7	11.1	<1sec

5.2.2 Ammonia sensing behaviour of ZnO thin film

Fig. 5.3(a) and (b) shows the sensitivity (%) of the as-deposited (S1) and rapid thermal annealed (RTA) ZnO thin film (S2) at different concentration of ammonia. Ammonia concentration has been varied from 50 ppm to 1000 ppm. It has been observed that the sensitivity increased by increasing ammonia concentration for all the samples. Both as-deposited (S1) and RTA processed ZnO thin film (S2) have shown highest sensitivity for ammonia concentration of 1000 ppm, where as sensitivity of RTA annealed film 8.2 % was higher than that of as deposited film i.e. 6.1% at room temperature. This is attributed to the enhancement of surface area during RTA by evolution of the porous morphology as discussed in chapter 3. In annealed film,

ammonia easily penetrates towards the bulk of the film due to its porous nature and interacts with the more number of granular surfaces of the enhanced surface area. The exposure time to each of these samples was 40 s.

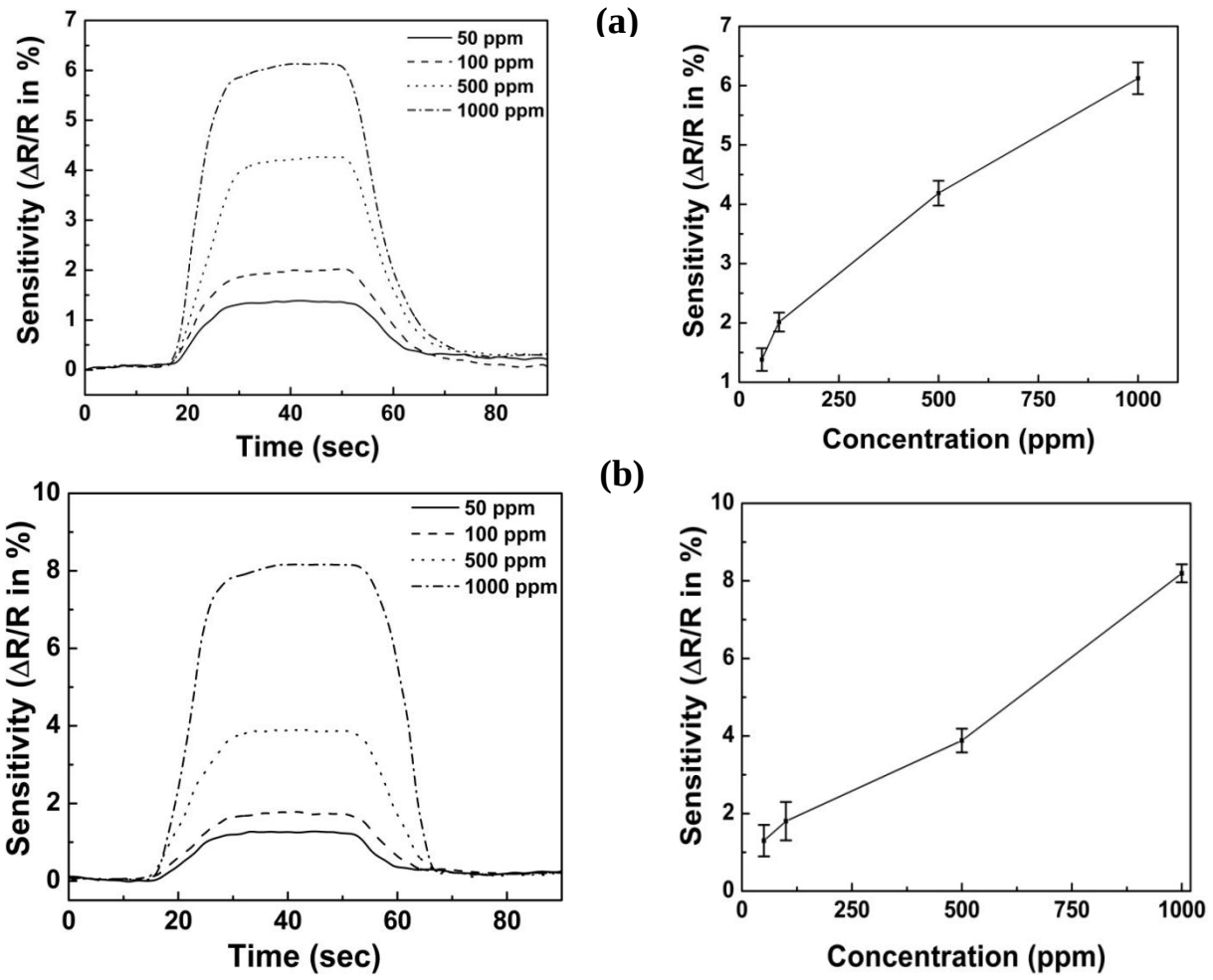

Fig. 5.3 Sensitivity plot of ammonia for (a) as-deposited (S1), and (b) rapid thermal annealed (RTA) (S2) ZnO thin film

5.2.3 Ammonia sensing behaviour of various ZnO nanostructures

Sensitivity of various ZnO nanostructures in presence of ammonia is shown in fig. 5.4. All the nanostructures show enhancement in sensitivity with an increase in ammonia concentration, which is attributed the reduction in the adsorbed surface oxygen. Thus, decrease in adsorbed oxygen concentration gives rise to increase of free electron. The variation of sensitivity with the concentration of ammonia at 1000 ppm for different nanostructures (nanowires, nanorods, nanoplatelets, nanoflakes) at room temperature is given in Table 5.1.

Fig. 5.4(a) shows the variation of sensitivity of ZnO nanowires (S3) at different ammonia concentration. The sensitivity of ZnO nanowires (S3) varies between 4 % and 46.3 % at room temperature for ammonia concentration of 50 to 1000 ppm. Fig. 5.4(b) shows the variation of sensitivity with various concentration of ammonia for ZnO nanorods (S4). The sensitivity of ZnO nanorods varies between 1 % and 16.9 % for 50 ppm – 1000 ppm of ammonia concentration at room temperature. For the nanowires (S3) and nanorods (S4), the sensitivity for 1000 ppm of ammonia is 46.3 % and 16.9 % respectively. Nanowires with high aspect ratio, leads to good sensitivity as compared to nanorods.

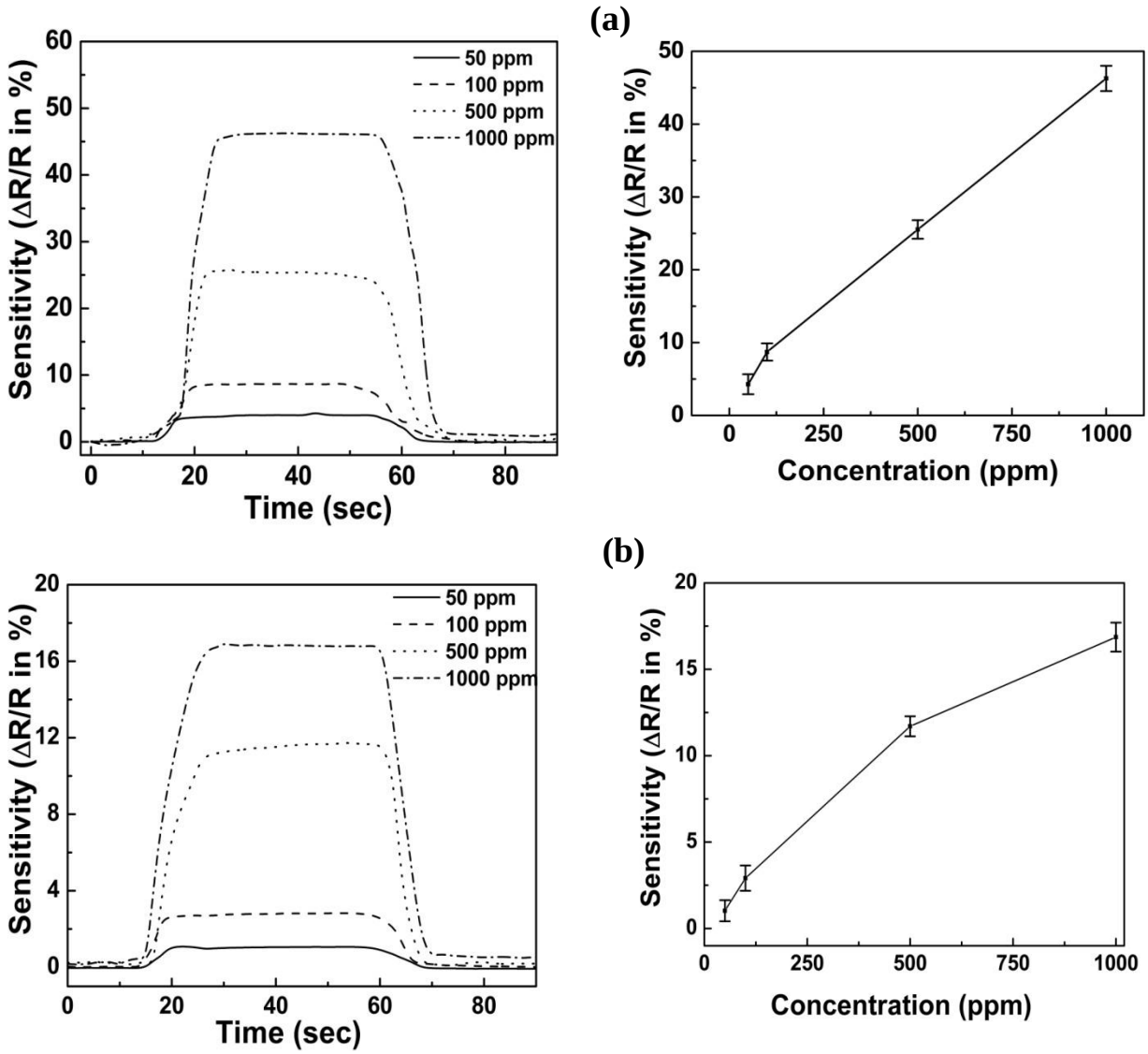

(d)

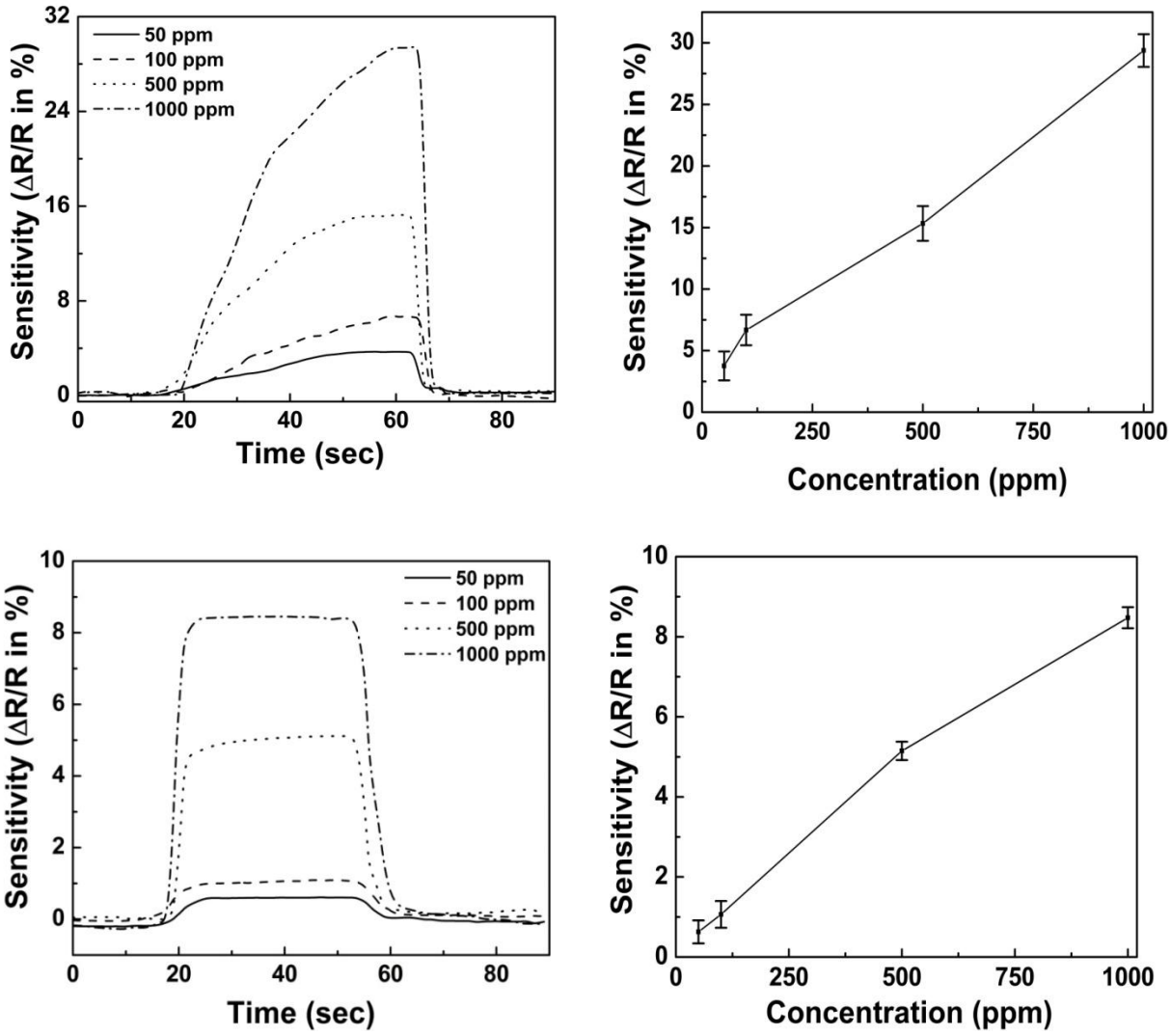

Fig. 5.4 Sensitivity plot of ammonia for various ZnO nanostructures (a) Nanowires, (b) Nanorods, (c) Nanoplatelets, and (d) Nanoflakes

nanoflakes (S6) with the variation in concentration of ammonia at room temperature. For various ammonia concentrations 50-1000 ppm, nanoplatelets (S5) and nanoflakes (S6) sensitivity lies in the range 3.7 % – 29.4 % and 0.6 % – 8.5 % respectively. It has been observed that nanoplatelets (S5) does not shows saturation behaviour [Fig. 5.4(c)]**,** which may be due to the presence of large number of surface states or trap centers, which limits the faster generation of the free electron [18-19]. On the other hand, these nanoplatelets (S5) show higher sensitivity than nanoflakes (S6) at 1000 ppm of ammonia concentration. Among the different nanostructures, highest response of 46.3% has been observed for nanowires (S3).

5.2.4 Ammonia sensing behaviour of ZnO network like porous structure

Fig. 5.5 shows the variation in sensitivity (%) of ZnO nanoporous structure (S7) with various ammonia concentrations. Sensitivity of the nanoporous structure is found to be in the range of 26 % - 73.7 % for 50 ppm to 1000 ppm of ammonia concentration at room temperature. The highest sensitivity of the porous structure is attributed to larger surface area and presence of less number of surface states or trap centers in the sample.

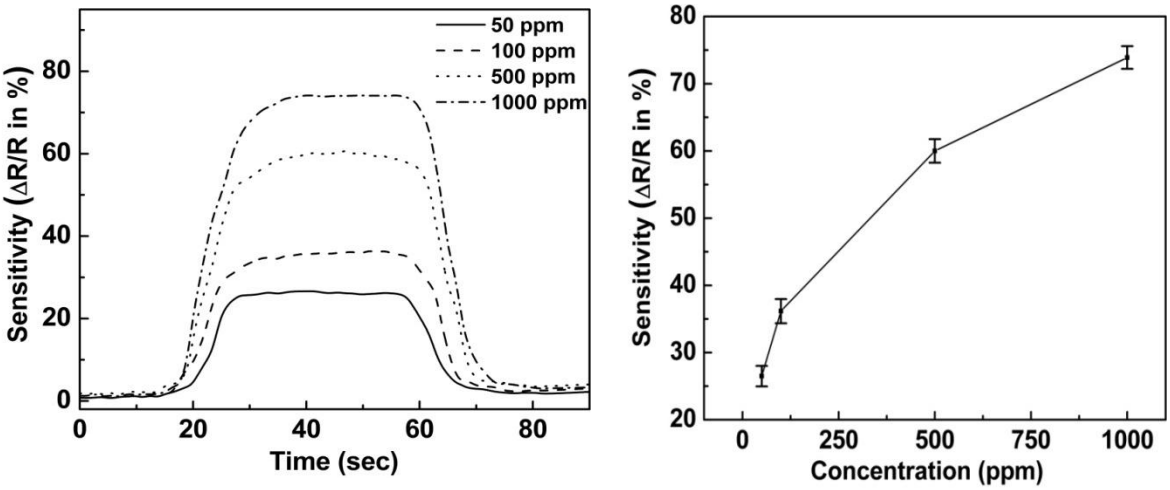

Fig. 5.5 Sensitivity plot of ammonia for ZnO network like porous structure

5.3 UV detection of zinc oxide thin films and nanostructures

5.3.1 UV detection mechanism

ZnO has wide bandgap of 3.37 eV and therefore, it is suitable for UV-light detector. Intrinsic defects of ZnO that is oxygen vacancies and/or zinc interstitials plays a vital role in UV detection mechanism. The conductivity of ZnO is extremely sensitive to UV light exposure. Basically, the photosensitivity in ZnO is regulated by chemisorptions of oxygen [20-23]. Fig. 5.6 shows the schematic diagram of UV detection mechanism of ZnO nanostructures. In the absence of UV light, oxygen molecules get adsorbed on the nanostructure surface as negatively charged ions by confining the free electrons, thereby create a depletion layer with low conductivity near the surface:

$$O_2(g) + e^- \rightarrow O_2^-(ads.) \qquad (3)$$

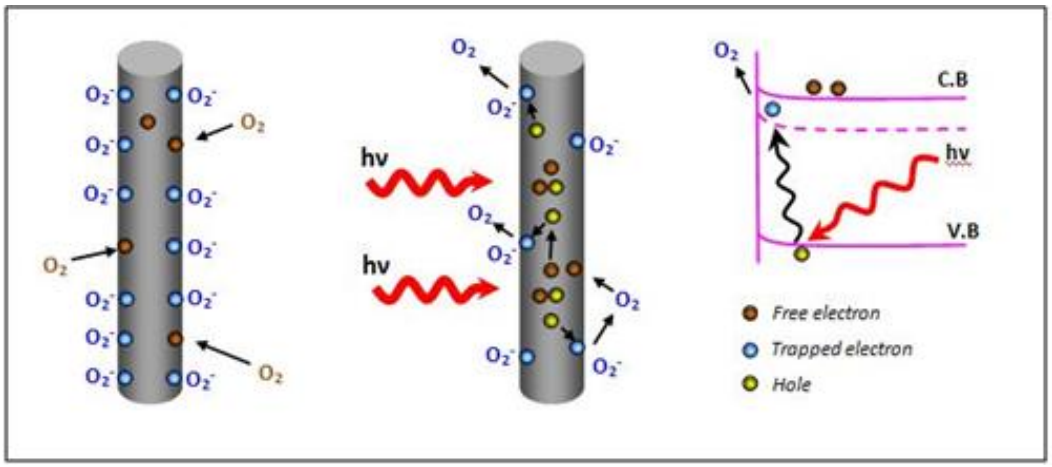

Fig. 5.6 Schematic diagram of UV detection mechanism of ZnO nanostructures [19]

When the sample is illuminated with UV light, whose photon energy is more than bandgap of ZnO, it causes generation of electron-hole pairs. Adsorbed oxygen ions combine with the holes to produce oxygen molecules, which desorbs from the NS surface. Under bias voltage, the unpaired electrons are collected at the anode, thereby an increase in conductivity takes place with the decrease in the width of depletion layer [24-26].

$$h^{+}(h\vartheta) + O_2^{-}(ads.) \rightarrow O_2 \qquad (4)$$

After completion of UV excitation, oxygen get readsorbed on the surface until equilibrium is restored. This readsorption is a slow process and significantly lengthens the relaxation time constant for the devices [27-32]. The slow transient can be expressed by a exponential function as [26]

$$I(t) = I_d + (I_p - I_d)\exp\left[-\left(\frac{t}{\tau}\right)\right] \qquad (5)$$

Where I (t) is the transient current, I_d is the current measured in dark, I_p is the current measured under UV illumination, t is the time after turning off UV light. Using exponential fit to the experimental data, the decay time constant (τ) can be calculated for all the samples. The details of the samples used for UV detection, are given in Table. 5.1.

5.3.2 UV detection of ZnO thin films

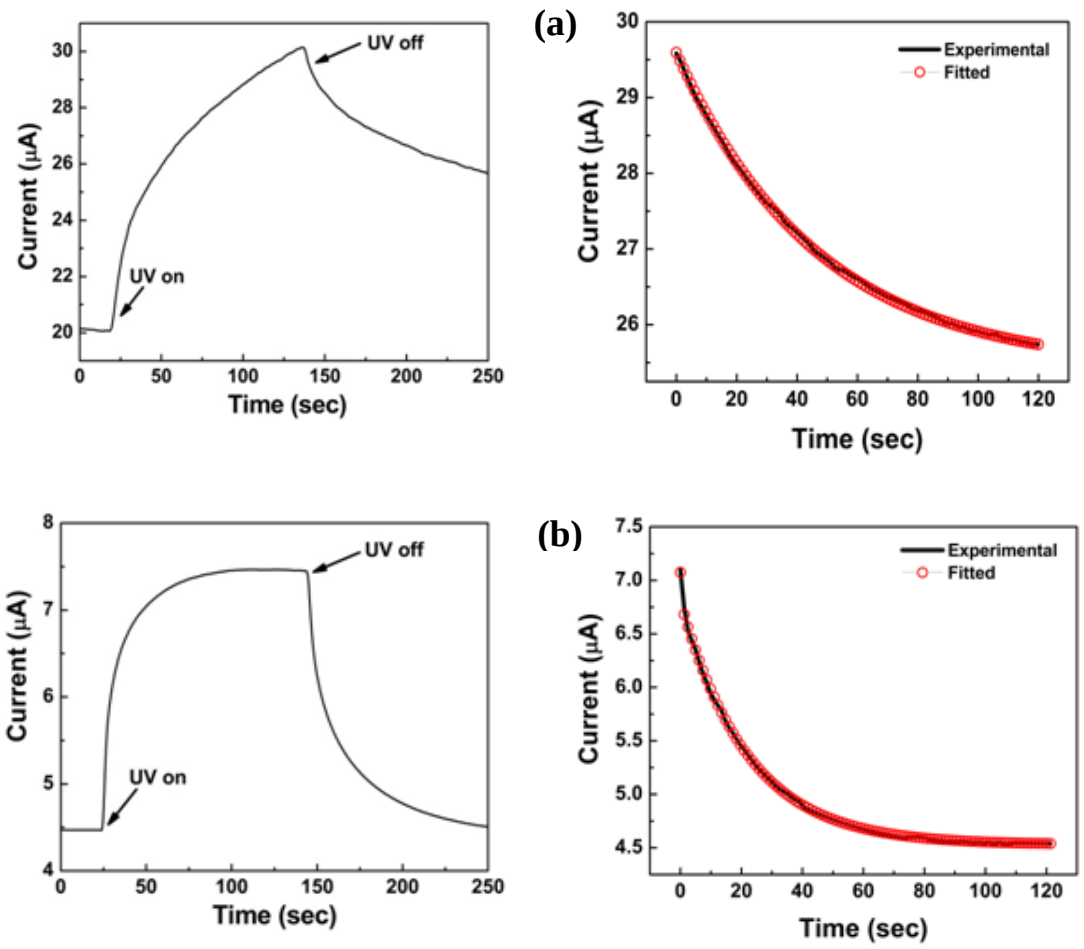

Fig. 5.7 Current-time and decay curve of (a) as-deposited (S1), and (b) RTA processed ZnO thin film (S2) under UV exposure

Fig. 5.7 (a) and (b) shows current- time and decay curve of (a) as-deposited (S1), (b) RTA processed (S2) ZnO thin film. The on/off ratio for the sample S1 is 1.5, whereas it is found to be 1.7. for S2. Fig. 5.7 (a) and (b) shows the transient photocurrent decay of samples S1 and S2 with decay time constant (τ) value of 47 s and 21 s, respectively. Annealed films have relatively lower decay constant (τ), which may be due to the faster evacuation of the charge carries. The relatively better response of sample S2 may be due to the annihilation of surface trap states during RTA process. In addition, the sample S2 has shown the quasi saturation of photo current.

5.3.3 UV detection of ZnO nanostructures

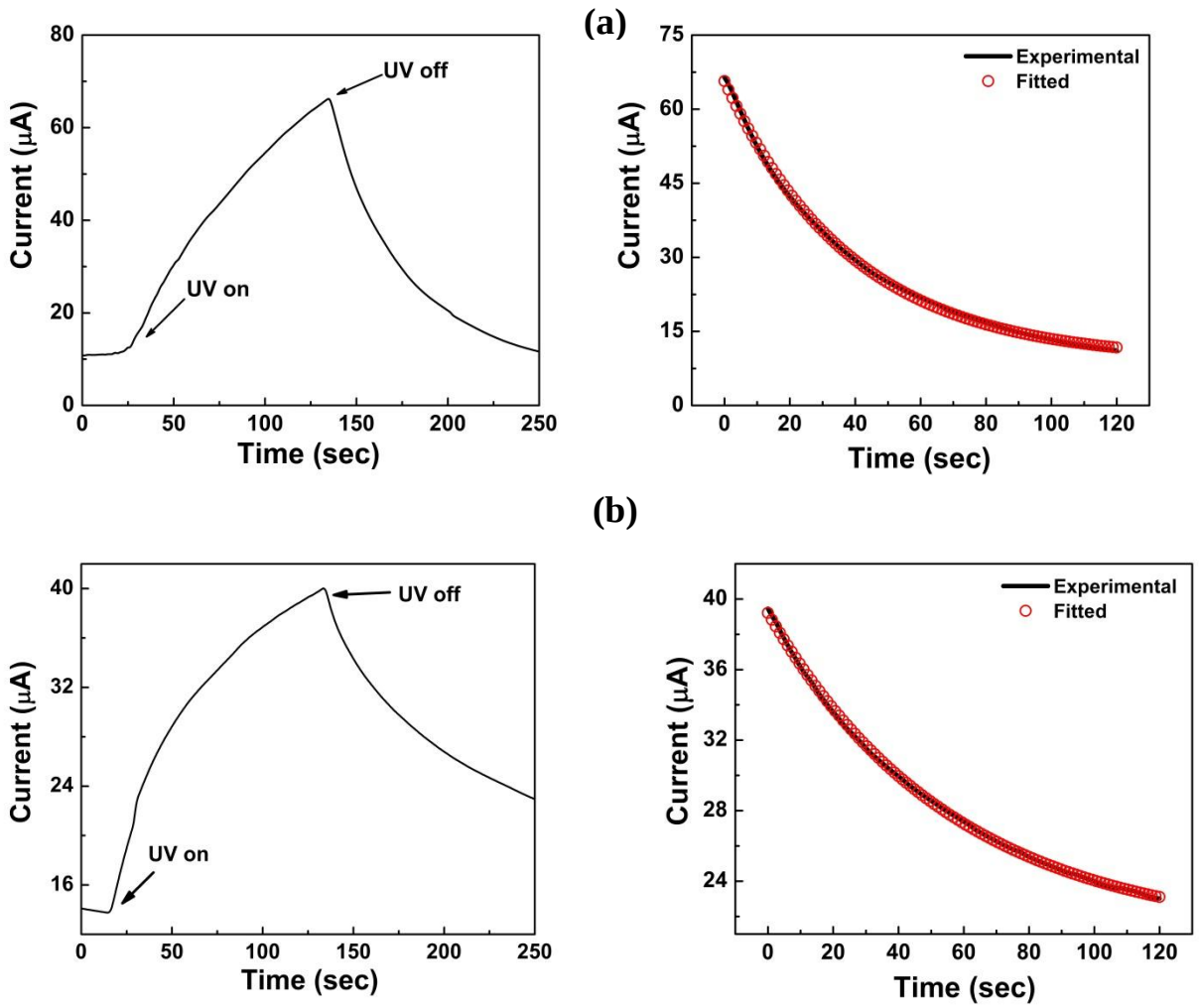

Fig. 5.8 Current- time and decay curve of (a) ZnO nanowires (S3), and (b) ZnO nanorods (S4) under UV exposure

Fig. 5.8 (a) and (b) shows current time and decay curve of ZnO nanowires (S3) and ZnO nanorods (S4) under UV excitation. The on/off ratio of ZnO nanowires (S3) photodetector is about 6.1, whereas it is found to be 2.9 for sample S4. From experimental results, the decay time constants τ_1 and τ_2 are estimated to be around 39 s and 57 s, respectively by fitting the decay curve using the exponential function. However, the photo current was not well saturated for both sample S3 and S4, which may be due to the presence of surface states in the aqueous grown nanowires/nanorods. Secondly, in case of nanorods (S4) the decay time constant is relatively

slow, which is attributed to delayed readsorption of oxygen molecules onto the nanorods surface due to its larger width.

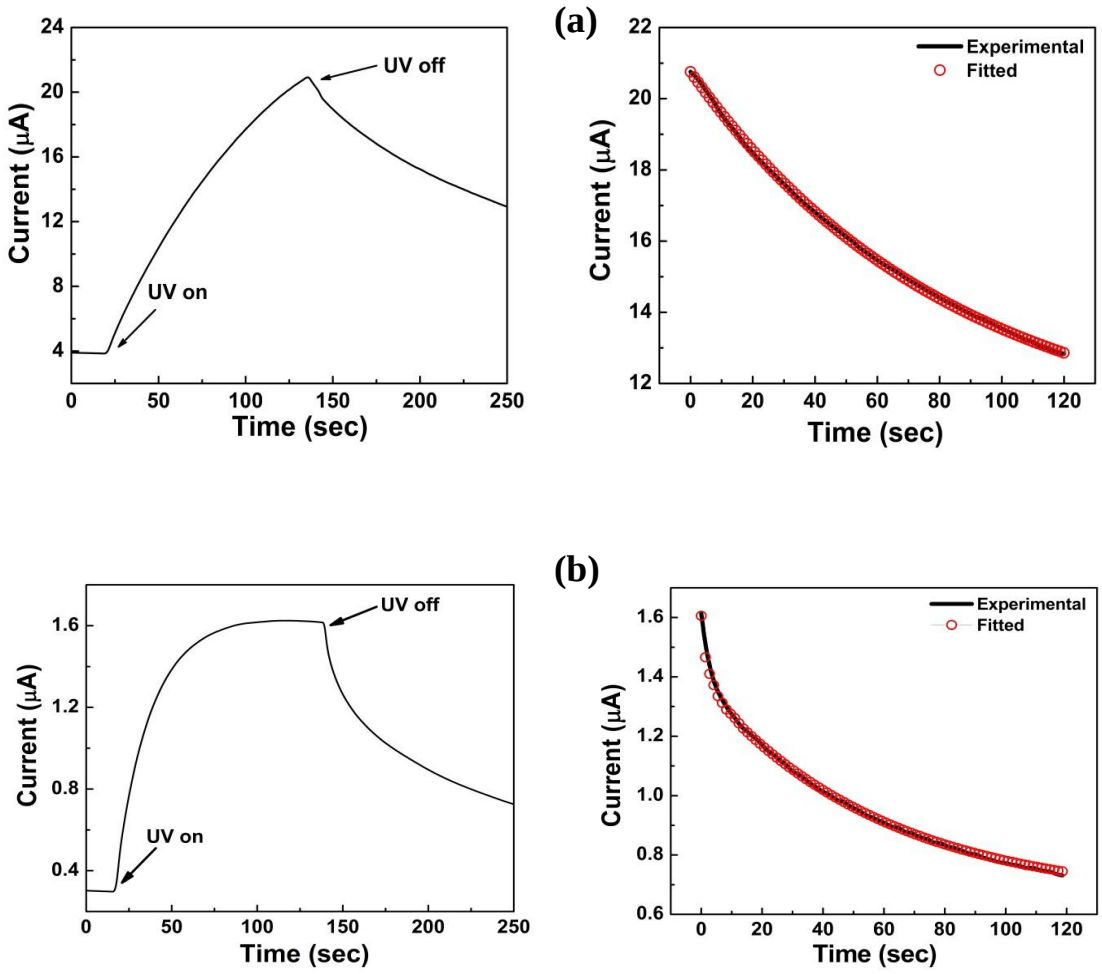

Fig. 5.9 Current-time and decay curve of (a) ZnO nanoplatelets (S5), and (b) ZnO flakes (S6) under UV exposure

Fig. 5.9 (a) and (b) shows the current-time and decay curve of nanoplatelets (S5) and nanoflakes (S6), respectively. The plot reveals the UV on/off current ratio of the nanoplatelets (S5) is 5.3. Furthermore, the on/off ratio of the sample (S6) was found to be 5.2. Nanopaltelets and nanoflakes are obtained by adding aluminium nitrate nonahydrate to the hydrothermal solution. As Aluminum has one more extra valence electron than zinc, it will lead to increase the carrier concentration of ZnO nanoplatelets/nanoflakes. This will result in contribution of more

free electrons to the conduction band thereby increasing the conductivity or photocurrent in nanoplatelets (S5) i.e Al 3 at. %. However, it has been observed that in case of nanoflakes (S6) with Al 5 at. %, there was reduction in photocurrent. This decrement may be due to excess of the thermodynamic limit of the solubility **[**33]. The photocurrent decay depends on the rate of adsorption of oxygen molecules on the ZnO nanostructure surface to capture excess electrons **[**34-35]. However, nanoflakes above shown better UV detection due to its quasi-saturated photocurrent and faster decaying nature in comparision to nanoplatelets.

5.3.4 UV detection of network like ZnO porous structure

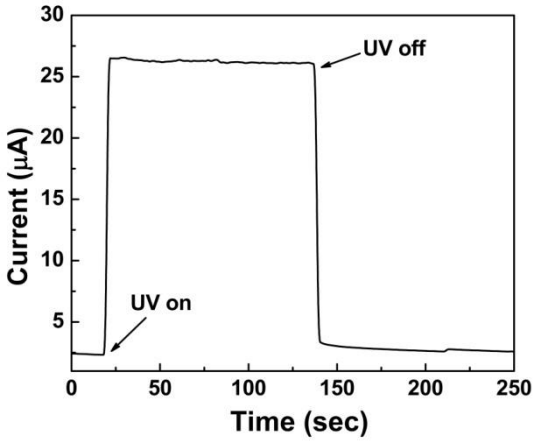

Fig. 5.10 Current- time measurement of network like ZnO porous structure under UV exposure

Fig. 5.10 shows the current-time measurement of network like ZnO porous structure (S7) under UV exposure. The sharp fall of the current, during turning on and off UV light, indicates fast response and recovery time for the ZnO porous photodetectors. The faster response and recovery time is attributed to the rapid adsorption and desorption of oxygen molecules. In addition, well saturated photocurrent indicates the better sensing ability of network like ZnO porous structure.

5.4 Chapter summary

This chapter focuses on the ammonia sensing behaviour and UV detection characteristics of ZnO thin film and nanostructures. The sensing of ammonia gas was performed in a gas

sensing chamber and the output were measured using Keithley current time measurement system. Annealed film has shown higher sensitivity than as-deposited film. Among different nanostructures the highest sensitivity has been observed for network like ZnO porous structure. Also, the porous structures have shown the faster decay time constant with high on/off ratio during the UV detection.

5.5 References

[1] C. S Rout, M. Hegde, A Govindaraj and CNR Rao, Nanotechnology **18** 205504 9 (2007).

[2] B. Timmer, W. Olthuis and A. Berg Sensors Actuators B **107** 666 (2005).

[3] H. Nanto, T. Minami and S. Takata, J. Appl. Phys. **60** 482 (1986).

[4] G. Sberveglieri, S. Groppelli, P. Nelli, A. Tintinelli and G. Giunta Sensors Actuators B **24** 588(1995).

[5] M. Aslam, V. A. Chaudhary, I. S. Mulla, S. R. Sainkar, A. B. Mandale, A. A. Belhekar and K. Vijayamohanan, Sensors Actuators A **75** 162 (1999).

[6] M. S. Wagh, G. H. Jain, D. R. Patil, S. A. Patil and L. A. Patil, sensors actuators B **115** 128 (2006).

[7] T. Tut, T. Yelboga, E. Ulker and E. Ozbay, Appl. Phys. Lett. **92** 103502 (2008).

[8] Z. G. Ju, C. X. Shan, D. Y. Jiang, J. Y. Zhang, B. Yao, D. X. Zhao, D. Z. Shen and X. W. Fan, Appl. Phys. Lett. **93** 173505 (2008).

[9] C. Soci, A. Zhang,B. Xiang, S. A. Dayeh, D. P. R. Aplin, J. Park, X. Y. Bao,Y. H. Lo, and D. Wang, Nano letters **74** 1003-1009 (2007).

[10] M. E. Swanwick, S. M. Pfaendler, A. I. Akinwande and A. J. Flewitt, Nanotechnology **23** 344009 (2012).

[11] J.G. Lu, P. Chang, Z. Fan, Mater. Sci. Eng. R **52** 49–91 (2006).

[12] A. Liu, Biosens. Bioelectron. **24** 167–177 (2008).

[13] Y. J. Chen, L. Nie, X. Y. Xue, Y. G. Wang and T. H. Wang, Appl. Phys. Lett. **88** 083105 (2006).

[14] Z. W. Chen, J. K. L. Lai and C. H Shek, Phys. Rev. B **70** 165314 (2004).

[15] P. Feng and Wang T H Appl. Phys. Lett. **87** 213111 (2005).

[16] Y. Chen, Zhu C L and Xiao G Nanotechnology **17** 4537 (2006).

[17] V. V. Sysoev, K. Bradly, B. K. Button, K. Wepsiec, S. Dmitriev and A. Kolmakov Nano Lett. **6** 1584 (2006).

[18] Ikram Ul Haq and Abdul-Majeed Azad, Sensors **12** 8259-8277(2012).

[19] K. Chongsri , and W. Pecharapa, Energy Procedia **56** 554 – 559 (2014).

[20] Y. Takahashi, M. Kanamori, A. Kondoh, H. Mimoura and Y. Ohya, Japan J. Appl. Phys. **33** 6611(1994).

[21] L. Liu, C. R. Goria, S. Liang, N. Emanetoglu, Y. Lu, H. Shen and M. Wraback, J. Electron. Mater. **29** 69 (2000).

[22] Chien-Yuan Lu, Sheng-Po Chang, Shoou-Jinn Chang,Ting-Jen Hsueh, Cheng-Liang Hsu, Yu-Zung Chiou and I-Cherng Chen, Semicond. Sci. Technol. **24** 075005 (2009).

[23] Mohamad Hafiz Mamat, Zuraida Khusaimi, Musa Mohamed Zahidi, and Mohamad Rusop Mahmood, Japanese Journal of Applied Physics **50** (2011).

[24] J. D. Prades, F. Hernandez-Ramirez, R. Jimenez-Diaz, M. Manzanares, T. Andreu, A. Cirera, A. Romano-Rodriguez and J. R. Morante, Nanotechnology **19** 465501(2008).

[25] Dong Chan Kim, Byung Oh Jung, Ju Ho Lee, Hyung Koun Cho, Jeong Yong Lee and Jun Hee Lee, Nanotechnology **22** 265506 8 (2011).

[26] S. Hullavarad, N. Hullavarad, D. Look and B. Claflin, Nanoscale Res. Lett. **4** 1421–1427 (2009).

[27] B. Claflin, D. C. Look, S. J. Park and G. Cantwell, J. Cryst. Growth **287** 16–22 (2006).

[28] R. Laiho, Y. P. Stepanov, M. P. Vlasenko and L. S. Vlasenko Physica B, **404** 4787–90 (2009).

[29] T. E. Murphy, K. Moazzami and J. D. J. Phillips, Electron. Mater. **35** 543–549 (2006).

[30] J. Nayak, J. Kasuya, A. Watanabe and S. Nozaki J. Phys. Condens. Matter **20** 195222 (2008).

[31] C. James Moore and V. Cody Thompson, Sensors **13** 9921-9940 (2013).

[32] A. Lalchand Patil, S. Lalita Sonawane, G. Dhanashri Patil, Journal of Modern Physics **2** 1215-1221(2011).

[33] M.H. Mamat, M.Z. Sahdan, Z. Khusaimi, A. Zain Ahmed, S. Abdullah, M. Rusop Opt Mat **32** 696-699 (2010).

[34] M.H. Mamat, Z. Khusaimi, M.Z. Musa, M.F. Malek, M. Rusop, Sensors and Actuators A **171** 241– 247(2011).

[35] Simas Rackauskas, Kimmo Mustonen, Terhi Jarvinen, Marco Mattila, Olga Klimova, Hua Jiang, Oleg Tolochko, Harri Lipsanen, Esko I Kauppinenand Albert G Nasibulin, Nanotechnology **23** 095502 7 (2012).

Chapter- 6

Conclusion and future scope

6.1 Summary of the results

This thesis focuses on the study of synthesis and characterizations of ZnO thin films and nanostructures on silicon substrates by modified aqueous chemical growth method for sensor applications. The first part of the work is concerned with growth and characterization of ZnO seed layer by optimization of different sputtering parameters such as RF power, substrate temperature, sputtering pressure and gas flow ratio. Secondly, in order to enhance the crystallinity of the film, post deposition heat treatment was done by using rapid thermal annealing system under various annealing conditions. Nanostructures of various morphology were fabricated using limited area heating of aqueous chemical growth. Finally, the investigation of ammonia sensing and UV detection behavior of ZnO thin films were studied by current-time measurement. Salient results of the thesis are concluded below.

ZnO thin films were deposited on n-type (100) silicon substrates by varying RF power from 75 W- 300 W and substrate temperature varied from room temperature to 300 ^{o}C. Highly crystalline c-axis oriented (002) peak has been observed for all the samples. The surface roughness was found to be decreased with increase in RF power, whereas films with bigger grains and higher roughness were observed at 300 ºC. The films, grown at the RF power of 150 W and substrate temperature of 200 ºC found suitable for the use of seed layer. After optimizing the RF power and substrate temperature, variation in sputtering pressure (1×10^{-2} - 4×10^{-3}) mbar and Ar/O_2 gas flow ratio (1:4 to 4:1) were made. Further, highly crystalline c-axis (002) oriented thin films are observed for lower sputtering pressure. The film deposited at lower working pressure has shown regular shape grains with uniform and homogeneous morphology. Investigation on gas flow ratio has shown smoother surface at $Ar:O_2$ flow ratio of 2:3, whereas the optimized pressure was found to be 4×10^{-3} mbar. In addition, $Ar:O_2$ flow ratio of 2:3 has shown highly crystalline c-axis oriented (002) plane.

Post-deposition rapid thermal annealing (RTA) was performed for improving the quality of RF sputtered ZnO film. Relatively high c-axis (002) oriented films were obtained at 1000 °C in air ambient for an annealing duration of 150 seconds. The surface of the films, annealed for 600 seconds, became rough due to the evolution porous microstructures, whereas the films annealed in oxygen ambient has shown smoother surface morphology. FTIR characteristic absorption peak of ZnO bond was found around 485 cm^{-1}. The characteristic absorption band of Zn-O became prominent due to the increase in Zn-O bond density by the oxidation of unbounded zinc atoms during the RTA process.

ZnO nanostructures of different morphology were grown under various conditions by using limited area heating of aqueous chemical growth. In order to obtain aligned nanostructures on silicon substrates, optimized ZnO film was used as a seed layer. It has been observed that the morphology of the ZnO nanostructures is significantly influenced by the variation in growth conditions of the aqueous method where zinc nitrate and hexamethyltetramine was used as a precursor. Aligned ZnO nanowires are obtained at growth temperature of 95 °C for 0.01M concentration, where as nanorods were obtained at 75 ^{o}C for 0.05 M precursor concentration. ZnO nanoplatelets/flakes like structure are formed on adding specific amount of aluminium nitrate nonahydrate in the above precursors. The vertical growth of ZnO nanostructures were limited by the formation of Al-complex on the polar surface of ZnO nanostructures. In addition, network like porous structure were obtained as a result of low temperature growth.

In order to make ohmic electrical contacts on the samples, thermal evaporation of aluminium using a shadow mask technique was performed. The ammonia sensing and UV detection of ZnO thin film and nanostructures were studied by performing current-time measurement. The sensitivity of all the samples was increased with increase in ammonia concentration. The annealed film shows better sensing property in comparison to the as-deposited one. Among different nanostructures, the highest sensitivity has been observed for ZnO network like porous structure. The porous structure has also shown the faster decay time constant of <1s with high on/off ratio during UV detection. The above experimental results can provide a platform in order to achieve room temperature operated next generation of metal oxide sensor.

6.2 Scope of the future research

The scope of the research on “Synthesis and characterizations of ZnO thin films and nanostructures by modified aqueous chemical growth method for sensor applications” are:

- Fabrication of single nanowire based sensor
- Surface functionalization with suitable chemicals
- Growth of long nanowire and TEM analysis
- Growth of nanoparticles by modified aqueous method
- Fabrication of FET and Schottky diodes for gas sensor using various nanostructures.
- Sensitivity measurment with different electrode spacing.

APPENDIX

Appendix-1

Material Properties of Zinc Oxide (ZnO)

Material Properties	Parameter Value
Molar mass	81.408 g/mol
Density	5.606 g/cm^3
Crystal structure	Hexagonal Wurtzite
Point group	6mm
Space group	P6$_3$mc
Melting point	1975 °C
Bandgap	3.37 eV (Direct)
Refractive index	2.0041
Exciton Binding Energy	60meV
Thermal conductivity	(0.6–1) Wcm^{-1}K^{-1}
Specific heat	40.3 J mol^{-1}K^{-1}
Intrinsic carrier	<10^6 cm^{-3}
Relative dielectric constant	8.656
Electron Hall mobility (300 K)	200 cm^2/V^{-1}s^{-1}
Hole Hall Mobility (300 K)	5-50 cm^2/V^{-1}s^{-1}

Sources:

1. Zhong Lin Wang, Rev. Phys. Chem., 55 (2004) 96-159.
2. Z. L. Wang, Z. C. Kang, Plenum press 465 (1998).
3. Z.L. Wang, J. Phys. Condensed Matter 16 829 (2004).
4. S. Lany, A. Zunger, Physical Review B. 72 35215 (2005).
5. Z. L. Wang, X. Y. Kong, Y. Ding, P. Gao, W. L. Hughes, R. Yang, and Y. Zhang, Adv. Funct. Mater. 14 943 (2004).

Appendix-2
List of equipments

Sl No.	Name of the Equipment	Equipment Model No.
1	Co- Sputtering	Excel - SPCH 12-3 Cust.
2	Thermal Evaporation	IHVP (12A4-D)
3	Spin Coating	Apex Spin-NXG P1
4	Rapid Thermal Annealing (RTA)	MTI Corporation
5	Current Voltage (I-V) Measurement	KEITHLEY (Picoammeter 6487)
6	Hot Plate with Magnetic stirrer	REMI (10MLH PLUS)
7	Ultrasonicator	LABMAN LMUC Series
8	Radio Frequency (RF) power supply	SEREN R601
9	Matching Network	SEREN NC2
10	Optical Microscope	RADICAL SCIENTFIC INST. (RXLr-4 Series)
11	X- ray Diffractometer (XRD)	RIGAKU JAPAN/ULTIMA-IV
12	Field Emission Scanning Electron Microscope (FESEM)	Nova NanoSEM/ FEI
13	Scanning Electron Microscope (SEM)	JEOL JSM-6084LV
14	Fourier Transform Infrared (FTIR) Spectrometer	Thermo scientific Nicolet 6700 system
15	Thin film Thickness Measurement	MProbe Thickness measurement System

Appendix-3

Cleaning procedure for silicon wafers

1. Ultrasonic cleaning in iso-propyl alcohol (IPA) bath-I for 5 minutes.
2. Ultrasonic cleaning in IPA bath- II for 5 minutes (ensure that the transfer from IPA- I to IPA- II should be quick and the liquid should not be allowed to evaporate from the wafer surface).
3. Ultrasonic cleaning in IPA bath-III for 5 minutes.
4. Through rinse in DI water by 5 changes of water baths with sufficient agitation.
5. Dip in 5 % HF solution for 30 seconds.
6. Thorough rinse in DI water.
7. $H_2SO_4 – H_2O_2$ (1:1 by volume) dip for 10 minutes.
8. Rinse thoroughly in DI water.
9. Repeat the step # 5 and # 8.
10. Spin dry of the wafers.

Publications

A. International Journals:

1. "Microstructural evolution of sputtered ZnO thin films with rapid thermal annealing", **S. P. Ghosh**, K. C. Das, N. Tripathy, G. Bose, T. I. Lee, J. M. Myoung and J. P. Kar. J. Mater. Sci: Mater. Electron. 26 (2015) 7860–7866.

B. Conferences:

1. "Fabrication of Aligned ZnO nanoplatelets using AlN film as an interfacial layer", **S. P. Ghosh**, K. C. Das, J. P. Kar, S. N. Das, G. Bose and J. M. Myoung, 17th National Seminar on Ferroelectrics and Dielectrics (NSFD), 17-19th Dec. 2012, SOA University, p- 43 Bhubaneswar.

2. "Morphological and Photoluminescence analysis of Zinc Oxide thin films deposited by RF sputtering at different substrate temperatures", **S. P. Ghosh**, K. C. Das, N. Tripathy, G. Bose, T. Lee, J. P. Kar, and J.M. Myoung, 4th National Conference on Processing and Characterization of Materials, 5th-6th Dec. 2014, National Institute of Technology, Rourkela. [IOP Publishing IOP Conf. Series: Materials Science and Engineering 75 (2015) 012023].

3. "Fabrication of porous ZnO thin films by rapid thermal annealing", **S.P.Ghosh**, K.C. Das, N. Tripathy, G. Bose, D.H. Kim, T. I. Lee, J. M. Myoung, J.P. Kar, International Conference on Multifunctional Materials for future Applications (ICMFA 2015), 27th-29th Oct. 2015, Indian Institute of Technology (IIT-BHU) Varanasi.

4. "Ultraviolet photodetection characteristics of Zinc oxide thin films and nanostructures", **S. P. Ghosh**, K. C. Das, N. Tripathy, G. Bose, D.H Kim, T. Lee, J. P. Kar, and J.M. Myoung, 5th National Conference on Processing and Characterization of Materials, 12th-13th Dec. 2015, National Institute of Technology, Rourkela.

5. "Influence of working pressure and oxygen Concentration on the Structural and morphological properties of ZnO films" **S.P Ghosh,** K. C. Das, N. Tripathy, G. Bose, D.H. Kim, T. Lee, J. P. Kar, and J.M. Myoung, 1st National Conference on Recent Advancement in Electronics (NCRAE)**,** 22nd-23rd Jan. 2016, IFHE, Hyderabad.

6. "Ammonia sensing behavior of ZnO Thin films and Nanostructures", **S.P Ghosh**, K. C. Das, N. Tripathy, G. Bose, D.H. Kim, T. Lee, J. P. Kar, and J.M. Myoung, 1st National Conference on Recent Advancement in Electronics (NCRAE), 22nd-23rd Jan. 2016, IFHE, Hyderabad.

BIOGRAPHY

Mr. Surya Prakash Ghosh was born in 1987 at Indore, Madhya Pradesh, India. He received his B. Sc. (Physics) in 2008 from North Odisha University and M. Sc. degrees in Physics from National Institute of Technology (NIT) Rourkela in 2012. Therefore,he has joined Master of Technology (Research) programme in Physics National Institute of Technology, Rourkela. His current research interests include fabrication and characterizations of semiconducting films/nanostructures for sensors and devices.